Erschienen in: Chemico-Biological Interactions. Elsevier. 2022, 351, 109766
https://doi.org/10.1016/j.cbi.2021.109766

Investigation of microcystin conformation and binding towards PPP1 by molecular dynamics simulation

Sabrina Jaeger-Honz [a], Jahn Nitschke [b], Stefan Altaner [b], Karsten Klein [a], Daniel R. Dietrich [b,1,*], Falk Schreiber [a,c,1,**]

[a] *Department of Computer and Information Science, University of Konstanz, Germany*
[b] *Department of Biology, University of Konstanz, Germany*
[c] *Faculty of Information Technology, Monash University, Australia*

Keywords:
Molecular dynamics simulation
Microcystin-LR
Microcystin congeners
Computational study
In-silico toxicology

A B S T R A C T

Microcystins (MC) are a group of structurally similar cyanotoxins with currently 279 described structural variants. Human exposure is frequent by consumption of contaminated water, food or food supplements. MC can result in serious intoxications, commensurate with ensuing pathology in various organs or in rare cases even mortality. The current WHO risk assessment primarily considers MC-LR, while all other structural variants are treated as equivalent to MC-LR, despite that current data strongly suggest that MC-LR is not the most toxic MC, and toxicity can be very different for MC congeners. To investigate and analyse binding and conformation of different MC congeners, we applied for the first time Molecular Dynamics (MD) simulation to four MC congeners (MC-LR, MC-LF, [*Enantio*-Adda5]MC-LF, [β-D-Asp3,Dhb7]MC-RR). We could show that ser/thr protein phosphatase 1 is stable in all MD simulations and that MC-LR backbone adopts to a second conformation in solvent MD simulation, which was previously unknown. We could also show that MC congeners can adopt to different backbone conformation when simulated in solvent or in complex with ser/thr protein phosphatase 1 and differ in their binding behaviour. Our findings suggest that MD Simulation of different MC congeners aid in understanding structural differences and binding of this group of structurally similar cyanotoxins.

1. Introduction

Microcystins (MC) are a diverse family of potent cyclic cyanotoxins occurring in mixtures in water bodies around the world [1]. Currently, there are at least 279 structural variants of MC described [2]. MC have been shown to be toxic to cattle [3–5], dogs [6,7] and other mammals [8–10]. Human exposure is frequent by accidental or deliberate ingestion of contaminated water, food [11–13], and food supplements [14,15], but also due to inhalation of aerosolised toxins [16]. Most notably, parenteral exposure of dialysis patients to contaminated water has highlighted the toxic potential of MC [17–19]. In addition, MC are suspected to cause long-term damage in multiple organs, as for example, liver, kidney and brain, when consumed repeatedly over a long-time scale [20].

The risk assessment by the World Health Organization (WHO) was conducted in 2004, reviewed and updated in 2020 [21], whereby the focus remained on MC-LR, i. e. one structural variant of the currently 279 described. The provisional guideline accepts a provisional tolerable daily intake of 0.04 mg per kg of body weight. This guideline includes an uncertainty factor of 1000 explained by database limitations, particularly on chronic toxicity and carcinogenicity. This equals to a provisional 0.001 mg per liter threshold for total MC-LR (free and cell-bound) in drinking water [21]. This value is solely based on one 13-week toxicity study in mice [22]. Since toxicological data on other variants than MC-LR are not taken into account, the WHO suggests a provisional approach of expressing MC burden as concentration equivalents of MC-LR as measured by HPLC, or as toxicity equivalents of MC-LR as measured by a bioassay, for instance a mouse bioassay or a protein phosphatase bioassay [21]. In view of the fact that current WHO guidelines neglect the structural diversity of MC, a better understanding

; MC, Microcystins; GSH, glutathione; PPP, ser/thr protein phosphatase.

* Corresponding author. Department of Biology, University of Konstanz, Germany.
** Corresponding author. Department of Computer and Information Science, University of Konstanz, Germany.
E-mail addresses: daniel.dietrich@uni-konstanz.de (D.R. Dietrich), falk.schreiber@uni-konstanz.de (F. Schreiber).

[1] Shared senior authorship

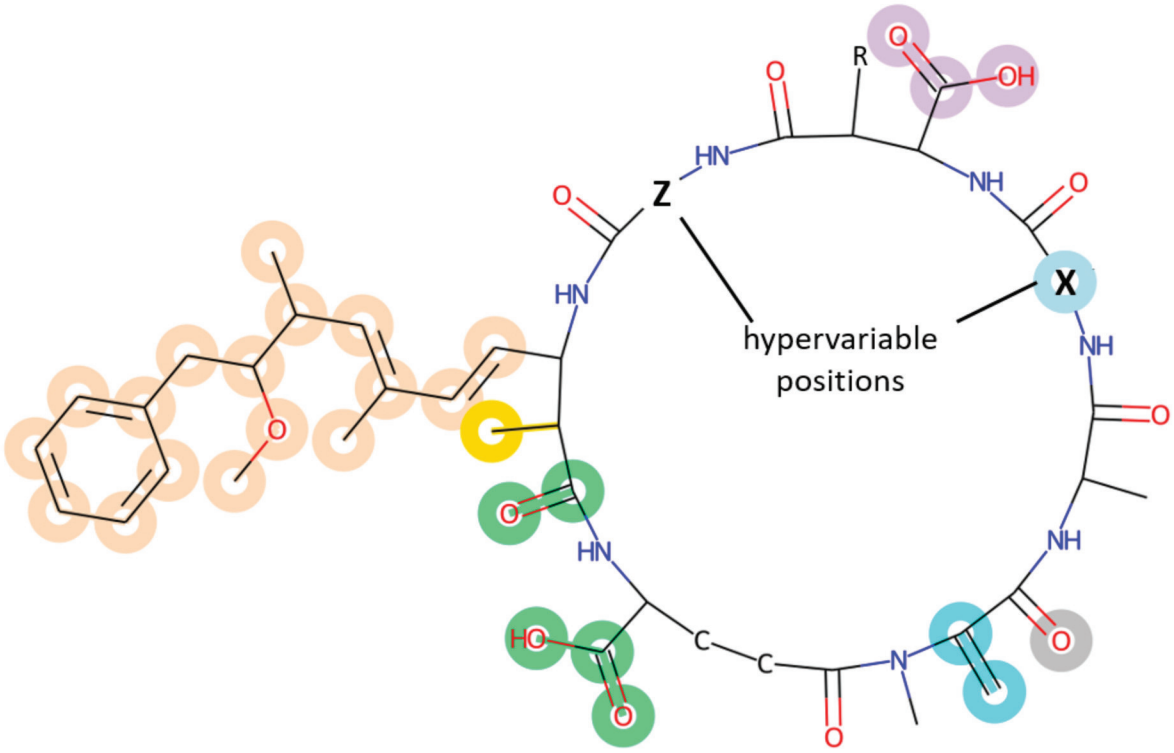

Fig. 1. Known interaction sites of MC with PPP1. X and Z denote hypervariable positions 2 and 4, which can be different amino acids. R can be a hydrogen or methyl group. The different types of interactions are indicated with different colours: Beige and light blue: hydrophobic interactions; gold: water molecule replacement; mint-green: indirect coordination to metals; cyan: covalent bonding; light purple: hydrogen bonds. Modified from Fontanillo and Köhn [38].

of toxicokinetics and –dynamics for different structural variants in humans is highly desirable and needed in order to develop a risk management strategy appropriately reflecting MC diversity.

Toxicokinetics and toxicodynamics of MC in humans, and other organisms, are defined by several protein-ligand interactions, which can vary greatly depending on the MC congener structure and on protein interaction partners [23]. In toxicokinetic studies with human or humanised *in vitro* systems, MC-LR has been shown to be taken up by organic anion polypeptide transporters of the human OATP family OATP1B1, OATP1B3 and OATP1A2 [23,24], of which the first two are expressed in the liver and the latter at the blood-brain barrier [25–27]. Moreover, the transport of MC congeners across the cell membrane highly depends on the affinity of the specific MC congener to a specific transporter type and the presence of other potentially competitively binding MC congeners [23]. In contrast to MC uptake, export mechanisms of MC congeners are not well investigated, albeit bidirectional transport by OATPs as well as unidirectional transport by MRPs could play a major role [28]. MC and different conjugates (cysteine (Cys) and glutathione (GSH)) are exported from hepatocytes to the systemic blood circulation and bile, in consequence leading to a higher residence time within the body [28,29]. The toxicodynamics of MC congeners in humans, and other organisms, involves reversible and irreversible binding of protein phosphatases (PPPs, i. e. PPP1, PPP2A, PPP5, PPP6) [9,29–31] as well as modifications and conjugations by Cys or GSH, i. e. intracellular mechanisms leading to moieties with potentially higher or lower toxicity [32,33].

The chemical interaction to PPP1 has been theorised to be tripartite: The hydrophobic Adda chain orienting the molecule towards the hydrophobic groove and thus the binding pocket as the initial step, followed by stronger electrostatic interaction, primarily between double positively charged ions and negatively charged moieties of MC, followed by a covalent bond between an unsaturated carbon atom of the methyldehydroalanine moiety in position 1 of the MC structure and the thiol of cystein 273 of PPP1 [34–36]. Inhibition of the PPP as a result of MC binding does not require the formation of a covalent bond [30,37]. Indeed, as defined, the non-covalent binding of MC to PPP1, albeit short-lived, is sufficient for PPP inhibition. However, while the non-covalent binding and thus inhibition of PPP is reversible, the covalent interaction is not, as extensively reviewed by Fontanillo and Köhn [38] and summarised in Fig. 1.

The nomenclature of MC considers variable features in the structure and uses the one-letter amino acid code (see Fig. 1) [39]. MC-LR, for example, has the L-amino acids leucine and arginine in the hypervariable positions 2 and 4 of the seven amino acid macrocycle. In contrast, the five remaining D-amino acids of the MC macrocycle, e. g. the Adda D-amino acid specific to MC and closely related nodularins, are present with very little modification in the majority of structural variants known to date [40]. Macrocycles represent, in many examples, ligands that behave differently from acyclic molecules. Often, macrocycles are conformationally restricted, possibly providing them higher affinity to target molecules since a bioactive conformation is entropically favoured [41]. Indeed, it has been reported that the simulated conformation of MC-LR in physiological water condition (transferable intermolecular potential with 3 points, TIP3P) was similar to the protein-bound bioactive conformation [35]. Due to the latter observation, the large size and the macrocyclic backbone, providing a scaffold for side-chains, these macrocycles could be interesting for drug development either as active moiety or as a vehicle [41,42].

To investigate differences in binding and conformations of MC, one computational method to apply is Molecular Dynamics (MD) simulation [43]. Due to the aforementioned scaffold function of a macrocycle, the structural variance of different MC congeners could be crucial for the protein interactions defining the toxin's toxicokinetics and toxicodynamics. Since the predominant interaction of MC in a cell impacting toxicodynamics is PPP1 inhibition, we employed MD simulations to investigate binding of four well-chosen MC congeners to PPP1. To the best of our knowledge, the most recent MC-LR conformational study via MD simulation was carried out in 1996 [44], while a MD simulation of

Table 1
Microcystin congener data set with IC_{50} values [29].

molecule	IC_{50} (nM)	Toxicity classification
MC-LR	0.3	Toxic
MC-LF	1.2	Toxic
[*Enantio*-Adda5]MC-LF	-[a]	Non-toxic
[*β*-D-Asp3, Dhb7]MC-RR	62.0	Less toxic

[a] Value is too high to be measured.

the PPP1-MC-congener interaction to explore MC toxicity was carried out in 2000 [35]. Other computational studies focused on modelling the covalent binding of MC to PPP1 [45], investigating the adsorption mechanism of MC at water-mineral interface [46], metal-binding selectivity and coordination [47], or on MC-LR and transformation products [48]. In view of the recent technical progress and more powerful approaches, i. e. a MD simulation approach of MC binding to PPP1 to determine differences in binding and conformation of four different MC congeners rather than restricting ourselves to MC-LR only was considered timely and advantageous. The MC congener structures were chosen to cover a wide range of PPP1 inhibition capacity as determined by a colorimetric phosphatase assay (see Table 1) [29]. Based on *in vitro* data, MC-LR and MC-LF belong to the most toxic known variants, whereas [*β*-D-Asp3,Dhb7]MC-RR is a natural congener showing lower toxicity *in vivo* and *in vitro* as well as a lower inhibitory potential of human PPPs. The fourth congener is [*Enantio*-Adda5]MC-LF, a synthetic enantio-variant of MC-LF which was shown to be non-toxic *in vitro* and lacking PPP1 inhibitory activity [49].

In the data presented, two MD simulation approaches were chosen: 1) a complex simulation to determine possible different binding modes and interactions and conformations of MC congeners with PPP1 and 2) a TIP3P (solvent) simulation to explore the unbound structure and macrocycle backbone behaviour of MC.

2. Methods

2.1. Data set

To cover a wide range of inhibition capacity of PPP1, four MD congener structures were chosen (see Table 1). IC_{50} values were determined by a colorimetric phosphatase assay by Altaner and coworkers [29]. Two of the most toxic known variants are MC-LR and MC-LF. [*β*-D-Asp3,Dhb7]MC-RR is a natural congener, which is less toxic, *in vitro* and *in vivo*, compared to MC-LR and MC-LF. [*β*-D-Asp3,Dhb7] MC-RR has two arginines at hypervariable positions 2 and 4 and in addition is demethylated at residue 3 (R = hydrogen, see Fig. 1) with an additional methyl group attached to the unsaturated carbon at residue 7 (at the atom coloured cyan). The fourth congener chosen was [*Enantio*-Adda5]MC-LF, a synthetic enantio-variant of MC-LF which is essentially non-toxic *in vitro* and lacking PPP1 inhibitory activity [49]. The stereochemistry of the Adda side chain (residue 5) of the [*Enantio*-Adda5]MC-LF is inverted at its four stereocenters.

2.2. Molecular docking

Based on the crystal structure of the PPP1-MC-LR complex in the protein data bank [50], all molecular dockings with the other MC-congeners were generated using the latter complex structures.

2.2.1. Preparation of PPP1

The asymmetric subunit A of PPP1 (PDB: 1fjm [51]; rPP1a) was used as receptor. All water molecules were excluded, except for two water molecules which coordinate metal ions in the active center. The charges of the respective water molecules were determined separately by computing the Gasteiger partial charges using UCSF Chimera [52]. The charge for the coordinated manganese ions was fixed at +2 before calculating partial charges of coordinating water molecules. Previous to docking, explicit hydrogen atoms were added to the receptor structure using UCSF Chimera [52].

2.2.1.1. Preparation of MC congener structures. The MC-LR structure in the crystallised structure of PPP1 (PDB: 1fjm [51]) was detached from rPP1c by deletion of the respective bond. Furthermore, a missing carboxyl group at D-glutamic acid was noted and considered an error. The carboxyl group was added manually using UCSF Chimera [52], the newly added bonds were energetically minimised using Chem3D® (version 16.0 by CambridgeSoft, PerkinElmer Informatics). The minimum RMS Gradient was 0.01, termination occurred after a maximum of 10 000 steps, heating temperature was at 0 K, target temperature at 300 K, the MM2 force field was used. Presumed structures of MC-LF, [*Enantio*-Adda5]MC-LF, and [*β*-D-Asp3,Dhb7]MC-RR were generated using the corrected MC-LR structure as a blueprint, since no reliable crystal structures of the respective congeners were available. To allow for the latter, features were added or deleted with UCSF Chimera [52] and displaced coordinates of stereoisomeric moieties were rotated around their stereocenters using Matlab R2016a [53] to generate [*Enantio*-Adda5]MC-LF from MC-LF. Prior to docking, explicit hydrogen atoms were added to all four ligand structures using UCSF Chimera [52].

2.2.2. Ligand-complex generation

Autodock 4.2 [54] was used to dock the respective congener structures to PPP1. The endpoint of the docking approaches was the comparison of the docked macrocycle backbone pose to the crystallised MC-LR structure (PDB: 1fjm [51], chain M in the asymmetric subunit A). This was done using the root mean-square deviation (RMSD) calculation function of UCSF Chimera. Each docking generated ten poses, which are by default sorted increasingly according to the docking score. Each structure was docked three times, yielding three sets of ten poses each. Since the program limits the total number of rotatable bonds to 32, the receptor, including manganese ions and water molecules at the active center, was treated as rigid. Additionally, Autodock 4.2 [54] is not reliably capable of treating a macrocycle as flexible, therefore the macrocycle backbone has to be treated as rigid. Indeed, all residues in MC congeners which differed among docked variants were kept rotatable (L-leucine (residue 2), L-arginine (residue 4) and Adda (residue 5)) in docking approaches to determine the initial poses for MD simulations in a complex with PPP1. The latter generated poses were compared to the macrocycle backbone of the crystallised MC-LR pose with the closest structure used as initial starting position for MD simulation.

The center of the grid box was set close to the active center at (91.226, 23.163, 24.424) with dimensions of 30, 22.5, 18.75 Å (corresponding to 80, 60, 50 arbitrary length units, used by Autodock 4.2 [54] with a spacing of 0.375 Å). Non-transformed coordinates were used from the published structure (PDB: 1fjm [51]). The docking preparation, procedure and standard parameters were employed according to the user guide, except for not replacing charges in the receptor structure, since manganese ions and coordinating water molecules were parameterised manually.

2.3. Molecular Dynamics (MD) simulation

The complex structures of PPP1-MC generated by molecular docking and MC structures were used to set up an MD simulation. The procedure for MD simulation used is described as follows.

2.3.1. Preparation of PPP1

MolProbity [55,56] was used to prepare PPP1 structure by adding hydrogen bonds and flipping of asparagine, glutamine and histidine. The terminal residues were modified, whereby N-methyl amide group (NME) and acetyl group (ACE) caps were added to the C- and N-terminal residues, respectively. For parameterisation of the protein structure,

Table 2
Summary of employed MD simulations and total simulation time.

Simulation type	System	Simulation time
solvent	MC-LR	20 ns
solvent	MC-LF	20 ns
solvent	[*Enantio*-Adda5]MC-LF	20 ns
solvent	[*β*-D-Asp3,Dhb7]MC-RR	20 ns
apo	PPP1	280 ns
complex	PPP1-MC-LR	280 ns
complex	PPP1-MC-LF	280 ns
complex	PPP1-[*Enantio*-Adda5]MC-LF	280 ns
complex	PPP1-[*β*-D-Asp3,Dhb7]MC-RR	280 ns

Amber ff14SB force field [57] was used and the active site waters were treated as TIP3P solvent. The default parameterisation of manganese ions in Amber ff14SB force field were not considered appropriate as this led to dissociation of manganese ions and active site water from PPP1 in the test runs of the simulation. For this reason, manganese parameters were exchanged with magnesium parameters. It was previously suggested that manganese ions have similar coordination preferences to magnesium ions and are only slightly larger [58]. Use of magnesium parameters lead to stable coordination of ions and active site water in the respective binding site of PPP1.

2.3.2. *Preparation of MC congener structures*

As MC congeners are macrocycles made up of non-standard amino-acids, these amino acids had to be parameterised manually before MD simulation. Thus for parameterisation, the non-natural amino acids were treated separately by splitting them from the macrocycle structure and capped with NME and ACE caps at the C- and N-terminus, respectively, to mimic an intact backbone. Hydrogens were added with UCSF Chimera [52], charges of different amino acids reported and calculations were set up on R.E.D. Server Development (see tutorial *IV*.1 central fragment of amino acid) to obtain charge derivation, force field library and force field parameters [59–62]. The quantum mechanical program used was GAMESS [63]. The charges were balanced and unknown parameters were derived from Amber ff14SB force field [57] or GAFF [64]. Parameters for standard amino acids were derived from the Amber ff14SB force field [57]. To generate topology files for each ligand, LEaP was used to obtain Amber topology files [65] and ParmEd [66] to translate file-formats for Gromacs topology.

2.3.3. *System preparation and setup*

MD simulations were performed with GROMACS version 2016.4 [67,68]. For each microcystin congener, a solvent simulation and a complex simulation was performed. In addition, apo simulations of PPP1 in solvent was set up.

For solvent simulation, a transferable intermolecular potential with 3 points (TIP3P) water model [69] was used. The system was neutralised with the respective amount of sodium ions. The particle mesh Ewald (PME) was applied with Verlet as cutoff scheme to allow calculation of long-range electrostatic interactions [70]. The LINCS algorithm was used to constrain bonds to their correct lengths [71]. Steepest descent minimization was performed with a maximum of 50 000 steps or until a maximum force smaller than 10.0 kJ/mol was reached. Subsequently, a NVT Equilibration was performed for 100 ps with a time step of 2 fs. The velocity-rescaling thermostat [72] was used to achieve constant temperature. This was followed by an NPT Equilibration of 100 ps to 1 bar with the Parrinello-Rahman barostat [73] and a step size of 1 fs prior the MD run. The MD run was performed for 20 ns with a step size of 2 fs. Three replicates were set up (see Table 2) for each MC congener - simulation type. For replicate 1, the docked structure of the ligand was used as the starting structure and PPP1 removed. For replicates 2 and 3, the snapshots of the ligand-solvent simulation of replicate 1 at 10 ns and 15 ns of the first simulation were used as the basic starting structure.

For complex and apo simulations the overall procedure is identical with the set-up for solvent simulation, except for: 1) step size of 2 fs for NPT Equilibration, and 2) the MD run was performed for 280 ns with a step size of 2 fs. As starting structures for replicate 1, the docked complexes of MC-congeners and PPP1 were used. For replicates 2 and 3 the protein structure of the apo simulations replicate 1 was extracted at 100 ns and 200 ns. These snapshots were subsequently aligned with the initial PPP1 structure of the docked complexes to generate new starting structures of MC-congener and PPP1 for replicate 2 and 3.

2.4. *Analysis*

Analysis was mostly performed with built-in tools from GROMACS [67,68]. To investigate the equilibration of the system, temperature and pressure were calculated over the whole trajectory. For further analysis of the trajectories, 30 ns and 5 ns were cut-off at the beginning of the trajectory for solvent and complex (and apo) simulation, respectively, to analyse the well-equilibrated trajectory. Periodic boundary conditions were removed and rotational and translational movements were eliminated by a least squares fit. To analyse changes in protein and ligand structure, the root-mean-square deviation (RMSD), volume, radius of gyration, and solvent accessible surface area was calculated. To estimate the binding of MC-congeners to PPP1, the number of contacts and hydrogen bonds were calculated. The backbone structures of PPP1 and MC congeners were analysed with Principal Component Analysis [74]. There are methods available to estimate binding free energies. Nevertheless, many approaches only offer an estimation of binding free energy (e. g. linear interaction energy) and require further fitting of parameters [75]. Since we focus on conformations and binding of MC congeners to PPP1, we did not further consider these approaches.

Python programming language was used to calculate properties and

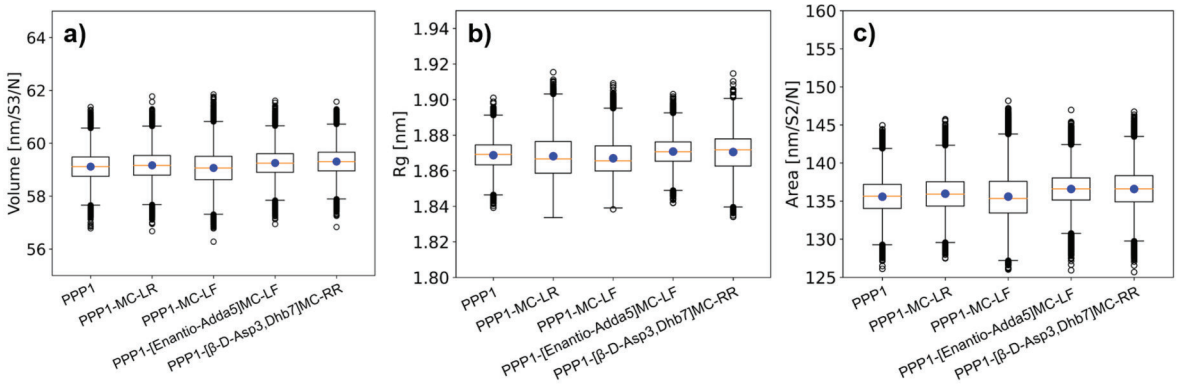

Fig. 2. Distribution of property values for PPP1 (with Mn^{2+} and active site water) during MD simulation. The median is marked with an orange line, while the mean value is shown as blue circle. The different properties to compare are: **a)** volume, **b)** radius of gyration and **c)** solvent accessible surface area of PPP1.

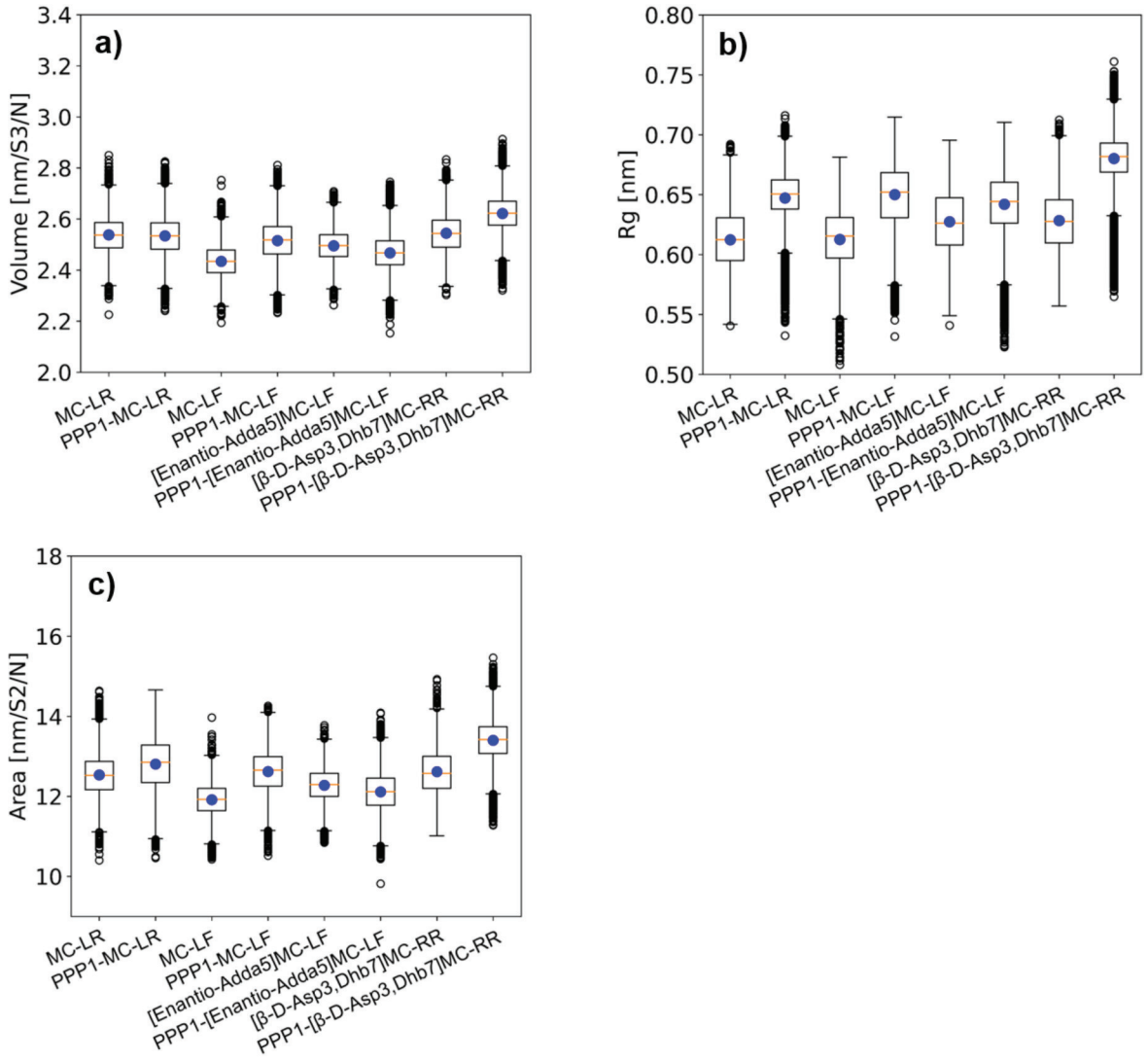

Fig. 3. Distribution of MC congener properties during MD simulation. The median is marked with an orange line, while the mean value is shown as blue circle. The MC congener properties compared are: **a)** the volume of MC congener in solvent simulation and complex simulation, **b)** the radius of gyration of MC congener in solvent and complex simulation, and **c)** the solvent accessible surface area of MC congener in solvent and complex simulation.

visualisations [76]. NumPy (version 1.18.5) [77] was employed to calculate mean values, standard deviation, median, and interquartile range. Boxplots were plotted with Matplotlib (version 3.2.2) [78] and a Mol2vec (version 0.1) helper function [79] was used for visualisation of principal component analysis. Jscatter, (version 1.2.7.2 [80]; a python module to simplify plotting with Grace [81]), was used for visualisation of time series data. Visualisations and images of the molecular interactions and structures during MD simulations were executed with PyMOL [82]. To compare the different simulation settings with each other, linear least-squares regression was applied for each simulation type (all replicates simultaneously) with SciPy function linregress. To quantify differences between different simulation types, a 95% confidence interval of slope and intercept was calculated as described in the SciPy reference guide [83].

3. Results and discussion

3.1. PPP1 stability

To investigate the influence of MC-congener binding on PPP1 structure, protein stability was investigated and compared to the PPP1 (apo) simulation. Upon MC-congener binding, we expected protein properties (volume, radius of gyration, solvent accessible surface area) to change in dependence of the respective MC-congener. The distribution of these properties over time is shown in Fig. 2, while mean, median and interquartile range values as well as statistical evaluation are provided in the Supplementary Information (see SI Table 1 and SI Table 2).

The distribution of the volume, radius of gyration and solvent accessible surface area of PPP1 is comparable for the different simulations (see Fig. 2). The radius of gyration is a measurement of the size and compactness of the protein. When considering the mean value (1.87 ± 0.01 nm) and median (1.87 nm), the radius of gyration did not change for PPP1. The latter suggested that the PPP1 structure was very stable throughout the simulation and did not change in size or compactness [84], irrespective of whether we simulated it as an apo structure or in complex with MC-congeners. Moreover, the volume of PPP1 was stable and did not change over time, with no significant differences in mean values observed (range: 59.07 $\frac{nm}{S^3/N}$ - 59.31 $\frac{nm}{S^3/N}$; see SI Table 1) for the different simulations. The solvent accessible surface area estimates how much of the protein surface is accessible to the solvent [85]. In line with volume and radius of gyration, the observed mean values for solvent accessible surface area (135.59 $\frac{nm}{S^2/N}$ 136.60 $\frac{nm}{S^2/N}$) are comparable for all simulations. The smaller the root mean squared deviation (RMSD), as

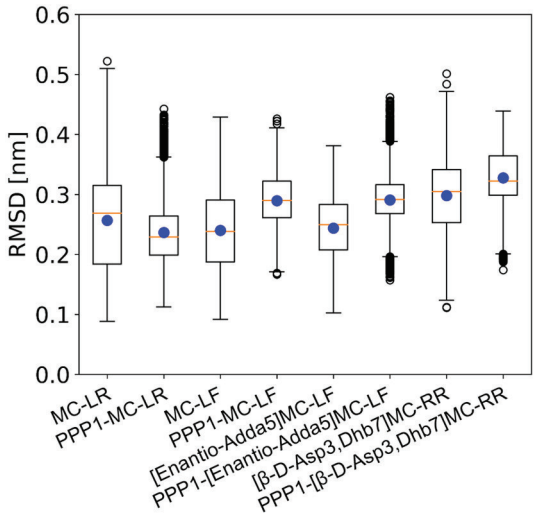

Fig. 4. Distribution of MC congeners root mean squared deviation (RMSD) during MD simulation. The median is marked with an orange line, while the mean value is shown as blue circle.The RMSD is shown for MC congener in solvent simulation and for MC congener in complex simulation.

the parameter highlighting the deviation of a structure from a reference structure during simulation, the higher the structure stability (in this case PPP1; see SI Table 1 and SI Fig. 1). Backbone RMSD median values for PPP1-MC-congener simulations were all lower (except for [β-D-Asp3, Dhb7]MC-RR) in comparison to PPP1 simulation. Nevertheless, the backbone RMSD values for PPP1-MC-congener simulations appeared more distributed (except for MC-LF), suggesting higher protein flexibility compared to the apo simulations.

To statistically evaluate potential differences between complex and apo simulations, linear least-squares regression was applied and a 95% confidence interval of slope and intercept determined (see SI Table 2). The confidence intervals for slope were 0.000 for all three properties and simulations, suggesting stable values of properties during the simulation. The confidence interval of the intercept overlapped for the different simulations performed over different properties (volume, radius of gyration and solvent accessible surface area) determined. For PPP1 backbone RMSD, overall considered as very stable, the intercept confidence interval showed overall higher RMSD values for less and non-toxic MC-congener when compared to apo simulations, while simulations with toxic MC-congeners resulted in lower RMSD values compared to apo simulations, confirming the limited movement and flexibility in the PPP1 backbone structure. Accordingly, the complex simulated with toxic MC-congeners appeared even more stable than the apo PPP1 backbone. Thus, MC-congener binding does not result in major conformational changes in the structure of PPP1.

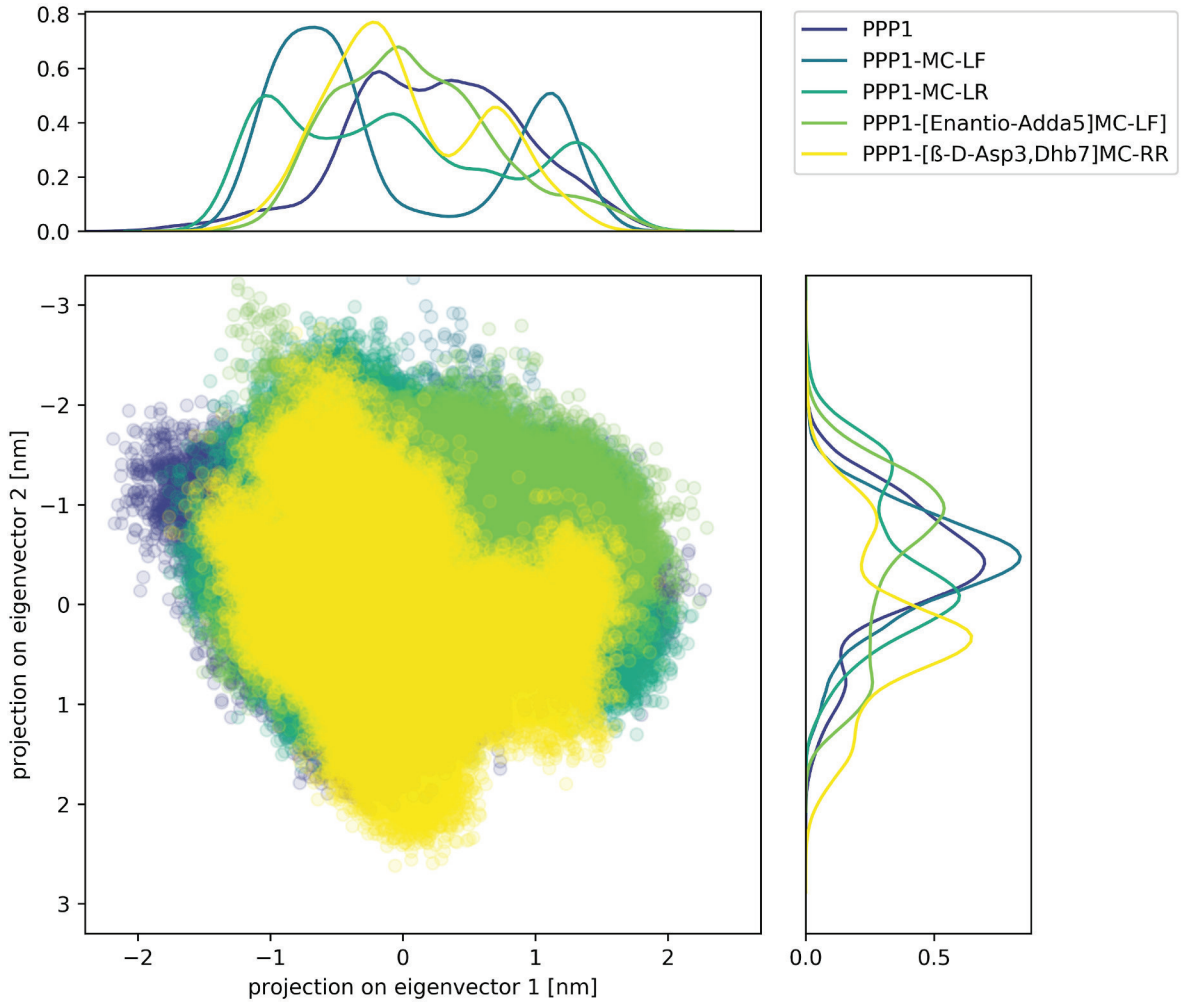

Fig. 5. Principal component analysis of PPP1 backbone of all complex MD simulations. The scatter plot is complemented by a distribution line, which shows the frequency of occurrence of a data point.

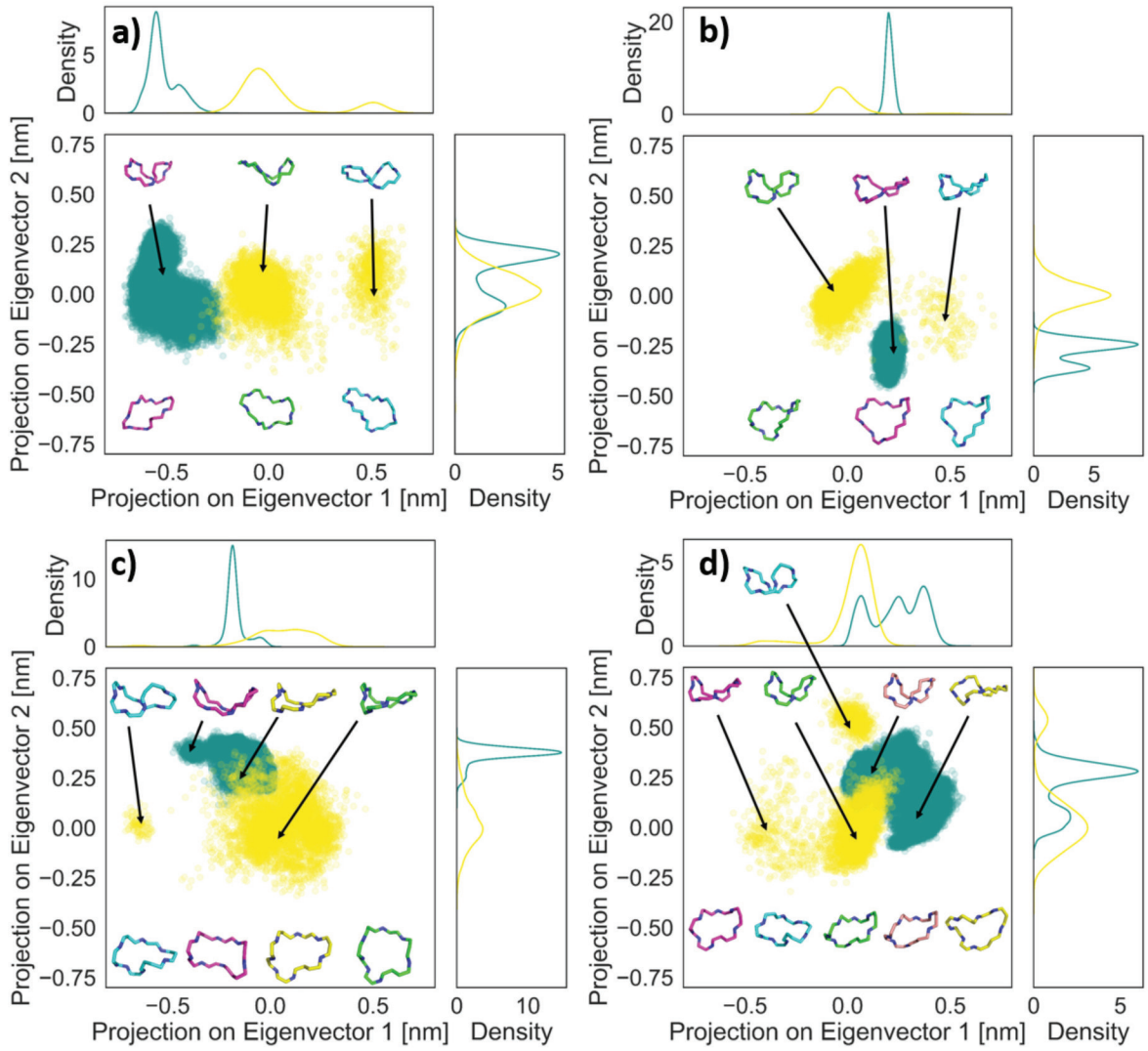

Fig. 6. Principal component analysis of MC congener backbone of complex (green) and solvent (yellow) MD simulations. The scatter plot is complemented by a distribution line, which shows the frequency of occurrence of a data point. In addition, the backbone structures of MC congener in the different clusters are shown as sticks. At the top the side view is visible, at the bottom the respective top view of each MC congener is shown. The MC congeners analysed are: **a)** MC-LR, **b)** MC-LF, **c)** [*Enantio*-Adda5]MC-LF, and **d)** [β-D-Asp3,Dhb7]MC-RR.

3.2. MC-congener stability

We also analysed the effect of PPP1 binding on the MC-congener macrocycle based on the volume, radius of gyration, solvent accessible surface area, and RMSD (see SI Table 3 and SI Table 4), i. e. corresponding to the approach taken to characterise the effect of macrocycle binding to PPP1.

The volume of MC congeners simulated in solvent compared to simulated in the PPP1 binding site is comparable for MC-LR, increased for MC-LF and [β-D-Asp3,Dhb7]MC-RR, and decreased for [*Enantio*-Adda5]MC-LF (see Fig. 3a). The radius of gyration (see Fig. 3b) and solvent accessible surface area (see Fig. 3c) is increased for all MC-congeners, except for [*Enantio*-Adda5]MC-LF,where the radius of gyration and solvent accessible surface area are comparable to the complex simulation. Even though most values are within their standard deviations, the distribution of values changes, as indicated by the boxplots in Fig. 3. These findings suggested that MC-congeners in general have a more open structure when binding to PPP1 than when simulated in solvent. This finding is expected, as MC-congeners have hydrophobic residues that try to shield from the hydrophilic environment in water and therefore result in a more coil-like structure than when compared to complex simulation with PPP1 binding. Indeed, it was described earlier that no major conformational change in backbone structure of MC-LR occurred when binding to PPP1 [44]. In contrast, [β-D-Asp3,Dhb7] MC-RR, being the most hydrophilic congener, attains a more open structure when binding to PPP1, which can be explained with the reduced interaction of [β-D-Asp3,Dhb7]MC-RR with the hydrophobic groove of PPP1. In addition, the values for volume, radius of gyration and solvent accessible surface area are in the same range as the other MC-congeners for solvent simulation, but when simulated with PPP1 in complex, we observe an increase in volume, radius of gyration and solvent accessible surface area with higher mean values for [β-D-Asp3, Dhb7]MC-RR, which is visible in Fig. 3. This is pointing towards a more open conformation of [β-D-Asp3,Dhb7]MC-RR when binding to PPP1 compared to other MC congeners. The latter interpretation is supported by statistical analyses (see SI Table 4) showing that volume and solvent accessible surface area of the more hydrophobic MC-LF and [*Enantio*-Adda5]MC-LF in solvent simulation is lower compared to MC-LR and [β-D-Asp3,Dhb7]MC-RR. Indeed, both MC-LF and [*Enantio*-Adda5] MC-LF have a phenylalanine (hydrophobic residue) at the hypervariable position 4. Even though the mean values for both congeners are within the standard deviation of each other, the values for [*Enantio*-Adda5]

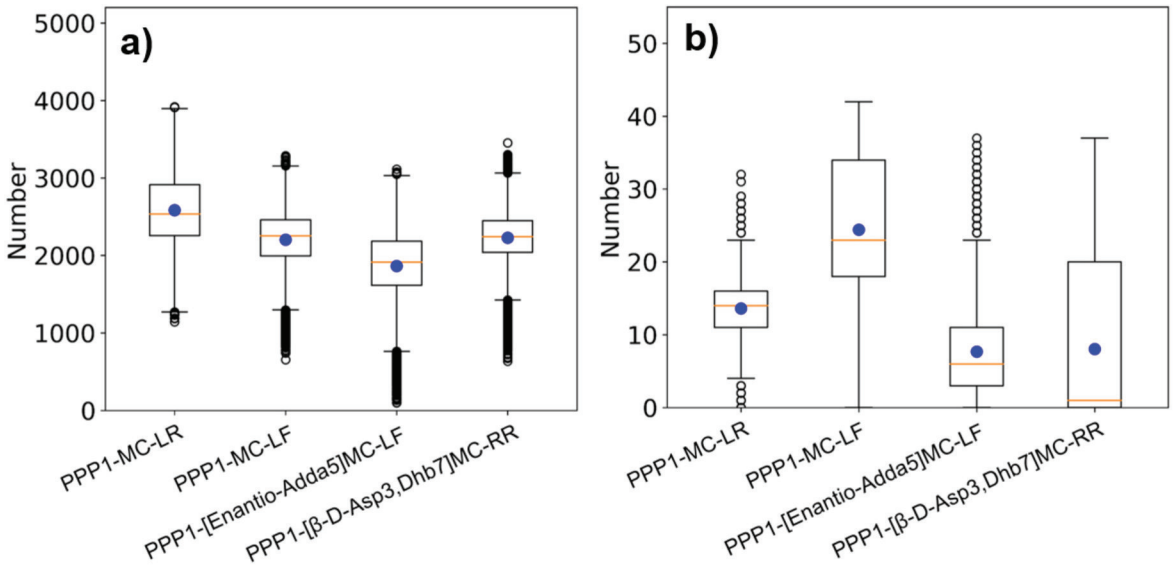

Fig. 7. Distribution of number of contacts (<0.6 nm) during MD simulation. The median is marked with an orange line, while the mean value is shown as blue circle. **a)** number of contacts between PPP1 and MC congener and **b)** number of contacts between Mn^{2+} and MC congener.

MC-LF are overall lower when simulated in complex with PPP1. This finding is explained by the orientation of Adda, which is flipped towards the backbone of MC instead of stretched as for MC-LF, due to the flipped stereocenters.

The all-atom RMSDs of the MC-congeners simulated in solvent and in the PPP1 binding site are shown in Fig. 4. In solvent, RMSDs were more widely distributed when compared to the simulations within the PPP1 binding site. The latter was expected, since the interaction with PPP1 limits the conformational space of MC-congeners. The all-atom RMSDs of MC-congeners simulations in complex with PPP1 results in higher all-atom RMSDs for all MC-congeners, which was also confirmed by statistical analysis (see SI Table 4). Interestingly, this change is smaller for MC-LR and resulted in an overall lowest RMSDs when compared to other MC-congeners. Whether the latter has any meaning with regard to intensity of MC-LR inhibition of PPP1 remains to be seen, although MC-LF was demonstrated to have a lower PPP1 inhibition capacity than MC-LR *in vitro* [29].

3.3. Analysis of conformational space

To determine the overall PPP1 backbone movement, principal component analysis (PCA) was performed (see Fig. 5). PCA is a mathematical method to project high-dimensional data in low-dimensional space to identify protein conformations [86]. The eigenvectors (principal components) of PPP1 backbone movement (apo simulations) were projected on the PPP1 structure of PPP1-MC-congener simulation, to allow for the comparison of the protein structure backbones with each other and observe differences to the apo simulations possibly caused by the interaction between PPP1 and MC-congener. The PCA projection of the apo simulations shows one big cluster, suggestive of a stable protein structure not prone to adopting different conformations, thereby confirming earlier findings above. PPP1-MC-LR (see SI Fig. 3) and PPP1-MC-LF (see SI Fig. 4) simulation provided for shifted distributions in comparison to the apo simulations (see SI Fig. 2) for both principal components. For PPP1-MC-LF two clusters are visible in the scatter plot and thereby suggest the presence of two major conformations. These cluster structures, however, overlap with PPP1-MC-LR and apo structure, and require further investigations to confirm whether this represents one major conformational cluster or two. The simulation with non-toxic congener PPP1-[*Enantio*-Adda5]MC-LF (see SI Fig. 5) shows a more narrow but comparable distribution to apo simulations. The latter suggests that PPP1 conformation is closer to the unbound state than when simulated with highly toxic congeners (MC-LR and MC-LF). The less toxic congener simulation PPP1-[β-D-Asp3,Dhb7]MC-RR (see SI Fig. 6) is also more comparable to apo than the highly toxic congener distribution, despite that principal component 2 (PC2) is shifted in comparison to apo simulations. To summarise, less and non-toxic MC-congeners have a comparable distribution along PC1, while they are shifted for PC2. The toxic congeners are shifted for PC1, but are comparable for PC2 in comparison to the apo structure. Overall, only one structural conformation is visible via PCA analysis, demonstrating that backbone stability of PPP1 is very high throughout all simulations, as discussed earlier for protein stability (see section PPP1 stability).

In view of the confirmed stability of the PPP1 backbone, various backbone conformations of the MC-congeners were analysed (see Fig. 6), basically representing various energy states attained [86]. Previous conformational studies of MC-LR led to the opinion that MC-LR backbone adopts to one saddle-shaped backbone conformation during MD-simulation in water [44] and in complex binding to PPP1 site [35]. The MC-LR simulation in solvent presented in this study, however, suggested two conformations to which MC-LR backbone can adopt (see Fig. 6a). Both conformations are comparable, nevertheless there is visible movement in the backbone of MC-LR. The cluster on the right in Fig. 6a represents the saddle shaped conformation described by Trogen et al. [44], while the majority cluster on the left (green stick) is also saddle shaped, albeit the backbone has adopted to a different shape. The right cluster (cyan sticks) is more sparsely populated than the cluster on the left, and only appears at the end of the third replicate, so additional simulations might be necessary to allow to discern whether this is a minor or a major cluster. Interestingly, the backbone structure changes when simulated with PPP1 according to PCA analysis. When looking in closer detail at the backbone conformation (pink sticks), the saddle shaped conformation is still visible, but seemed to be more skewed in comparison to the solvent backbone structure. Therefore, binding to PPP1 appeared to cause a small, but distinct change in MC-LR conformation, which had only a small overlap with the cluster of solvent simulation. The differences observed between the simulations results presented here and those reported in the literature may be in part due to the fact that we had simulated for a much longer time.

In contrast to MC-LR, MC-LF despite showing two clusters of backbone conformation in solvent simulation the second one is very sparsely populated (see Fig. 6b). The bigger cluster on the left (green stick) is

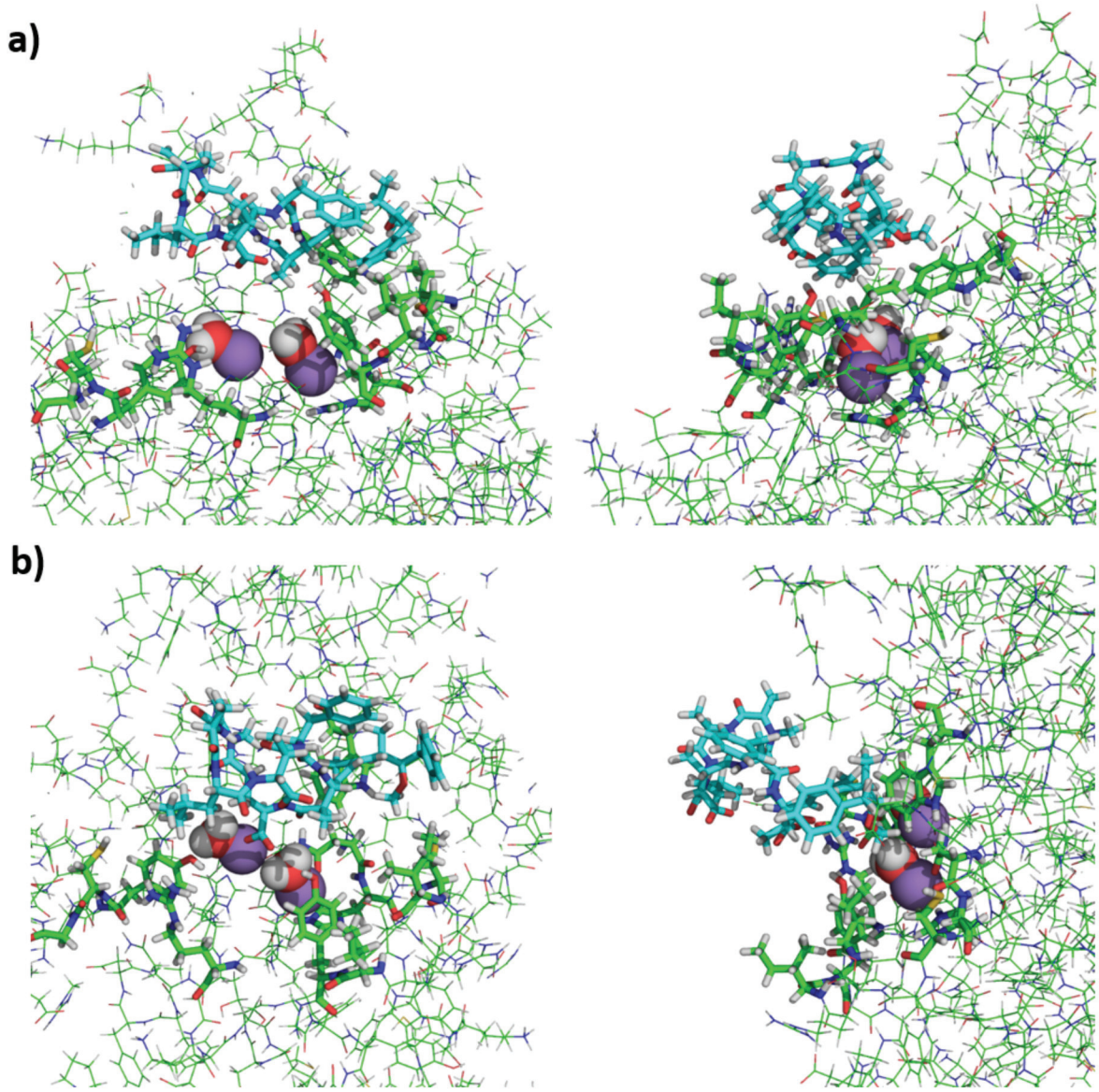

Fig. 8. Interaction of [*Enantio*-Adda5]MC-LF (cyan) with PPP1 (green). Known interacting residues are displayed in pink, interacting residues as lines in green. Mn^{2+} and the active site water is shown as spheres. Snapshots of the uncut trajectory to show binding of [*Enantio*-Adda5]MC-LF in the beginning of the simulation. **a)** Are snapshots at the beginning (top and side view) and **b)** (top and side view) towards the end of the uncut MD trajectory (first 30 ns).

more bent and pushed towards a more closed conformation, comparable to the backbone of MC-LR complex simulation. The small cluster on the right is sparsely populated (cyan stick) and has a different overall shape in comparison to the left cluster. The structures here mostly occur during the beginning of repetitions 1 and 2, thus suggesting that it is probably not as stable during solvent simulation as the bigger cluster on the left. The cluster of MC-LF backbone in complex simulation (pink sticks) is also completely shifted in comparison to solvent simulation, as was observed for MC-LR. The structure of the backbone is highly similar to the backbone structure of the sparsely populated cluster on the right. This is an indication that for MC-LF, as already observed for MC-LR, the backbone conformation in complex simulation does not change in comparison to solvent simulation.

In contrast to PCA analysis of MC-LR and MC-LF, [*Enantio*-Adda5] MC-LF and [β-D-Asp3,Dhb7]MC-RR have more overlap between the projection of solvent and complex simulation. [*Enantio*-Adda5]MC-LF (see Fig. 6c) backbone projection is distributed more widely in one big cluster and one smaller cluster in solvent simulation. Interestingly the major conformational cluster for solvent simulation with the backbone structure (green stick) is more similar to the backbone structure (cyan structure, see Fig. 6b) of MC-LF solvent simulation, while the backbone structure of [*Enantio*-Adda5]MC-LF in the minor cluster (cyan stick) is more similar to the backbone conformation of MC-LF (green stick, see Fig. 6b) in the major cluster. Nevertheless, the structures do differ in their conformation. The backbone projection of [*Enantio*-Adda5]MC-LF in complex simulation overlapped with the structure in solvent simulation. Moreover, where the clusters overlap, the structures were similar (green sticks in comparison to yellow sticks). Part of the cluster of complex simulation did not overlap with the major cluster of the solvent analysis. The backbone structure (pink sticks) was more bent in comparison, but still similar to the solvent structure. When we compared both pink structures of the complex simulation of [*Enantio*-Adda5]MC-LF and MC-LF with each other, the structures of the two MC-congeners appeared different. [*Enantio*-Adda5]MC-LF seemed to have a more closed conformation on the left side, while MC-LF was more open at this position.

For [β-D-Asp3,Dhb7]MC-RR (see Fig. 6d) PCA showed two clusters for solvent simulation and one scarcely populated one. The backbone

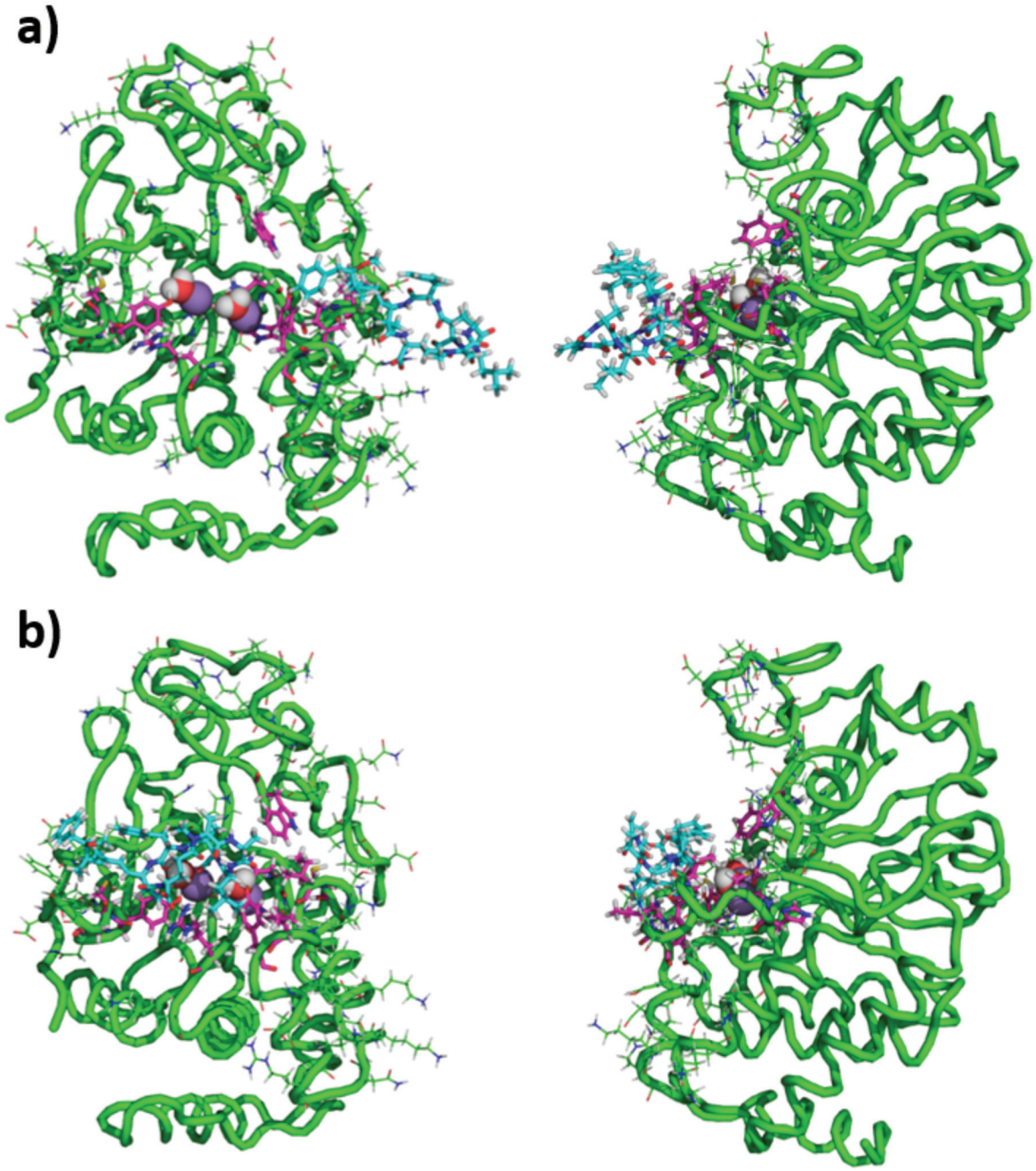

Fig. 9. Interaction of [*Enantio*-Adda5]MC-LF (cyan) with PPP1 (green). Known interacting residues are displayed in pink, interacting residues as lines in green. Mn^{2+} and the active site water is shown as spheres. **a)** Are snapshots at the beginning (top and side view) and **b)** at the end (top and side view) of the third replicate.

structure of the big solvent cluster (green sticks) was similar to the backbone structure of the scarcely populated cluster next to it (pink sticks). These clusters were close to each other and most likely belong together. The conformation of the second cluster at the top (cyan sticks) was on the right side different from the backbone structure in the major cluster (green sticks). The conformation of the loop at the back seemed to be oriented differently and more open. For the complex simulation, one big cluster was visible, but also here two structures were apparent. One, which overlapped with the solvent cluster (rose sticks) and one, which was located further away from the solvent cluster (yellow sticks). The overlapping structures were very similar with no difference observable when compared to the backbone structure in the major cluster (green sticks) of the solvent simulation. The representative backbone structure of the complex simulation (yellow sticks) had a less saddle-shaped conformation compared to the other structures, and was less bent. The latter observation was very interesting, as this was not observed for any of the other MC-congeners tested. The rather small modification of [β-D-Asp3,Dhb7]MC-RR, i. e. having a hydrogen instead of a methyl rest at position three, appeared to influence the overall backbone structure decisively, making it more flexible (also see SI Fig. 11 and SI Fig. 12).

3.4. PPP1-MC-congener binding

3.4.1. Quantitative analysis of binding

For molecular recognition, interactions between ligands (MC-congeners) and proteins (e. g. PPP1) are crucial. Important substructures of the ligand were delineated in Fig. 1. The Adda, in position 5, is reported

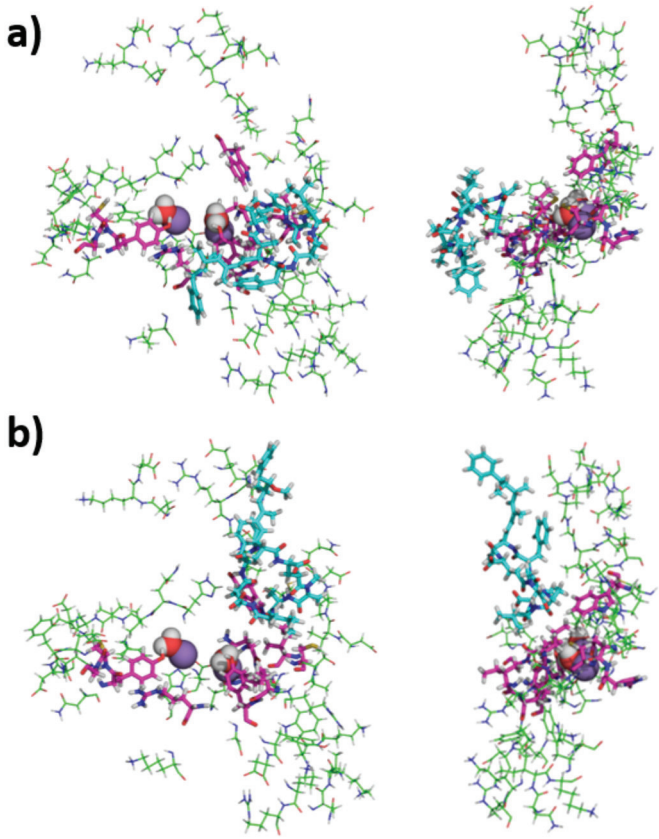

Fig. 10. Interaction of [*Enantio*-Adda5]MC-LF (cyan) with PPP1 (green). Known interacting residues are displayed in pink, interacting residues as lines in green. Mn^{2+} and the active site water is shown as spheres. **a)** Are snapshots at 89 ns (top and side view) and **b)** at 102 ns (top and side view) of the third replicate.

to be important for binding and building hydrophobic interactions with PPP1 [87]. Similarly, the amino acid at the hypervariable position 2 is also reported to provide for hydrophobic interactions. The carboxyl group at position 3 is capable of building hydrogen bonds [45], while the methyl rest in position 5 replaces water molecules in interaction, the carboxyl and carbonyl group at position 6 coordinate with the Mn^{2+} ions [51], and a covalent bond can be formed via the unsaturated methylene rest at position 7 [51,88]. However, as noted earlier, the covalent bond is not required for the inhibitive capacity, therefore obligatory tight interaction of the ligand (MC-congeners) with the protein (PPP1) was studied [38].

To investigate how well we were able to simulate the binding capabilities of MC-congeners to PPP1 by MD simulation, the number of contacts closer than 0.6 nm were determined (see SI Table 5). The number of contacts (<0.6 nm) are shown in Fig. 7a. The most toxic MC-congener MC-LR had the most contacts to PPP1 (mean value: 2583.77 ± 476.08, median: 2533), followed by MC-LF and [β-D-Asp3,Dhb7]MC-RR with a mean value of 2202.55 ± 370.54 and 2228.15 ± 335.82 and a median of 2252 and 2244, respectively. The non-toxic MC-congener [*Enantio*-Adda5]MC-LF had the lowest number of contacts to PPP1 with a mean value of 1863.62 ± 455.63 and a median value of 1913. Nevertheless, all number of contacts are within each others standard deviation, so this parameter is not suitable to distinguish between MC congeners, as it is a general observation of contacts between MC and PPP1 and does not distinguish for known interaction sites or the binding site.

The second important interaction for binding to PPP1 is the number of contacts (<0.6 nm) between MC-congeners (carboxylate anion, position 3) and Mn^{2+} ions, since it is known that this contributes to binding and subsequent PPP1 inhibition (see Fig. 7b). It was shown that when the carboxylate anion is removed at position 3, binding and subsequent inhibition is substantially reduced [89], which led to the assumption that the higher the number of contacts between Mn^{2+} ions, the better the binding of the MC congener would be. Interestingly, toxic congeners MC-LR and MC-LF have higher numbers of contacts with a mean value of 13.60 ± 4.02 and 24.42 ± 8.83 and a median of 14 and 23, respectively, than the less-toxic congener [β-D-Asp3,Dhb7]MC-RR (median of 1, mean value of 8.05 ± 9.99) and the non-toxic congener [*Enantio*-Adda5] MC-LF (mean of 7.69 ± 6.15 and a median of 6). Hence, we found a broad distribution of number of contacts (<0.6 nm) with an interquartile range of 0–20. We could show that the number of contacts between Mn^{2+} and [*Enantio*-Adda5]MC-LF, which is an important factor for binding and inhibition, was lower than for the highly toxic congeners, especially when comparing to its enantiomer MC-LF. The number of contacts between [β-D-Asp3,Dhb7]MC-RR and Mn^{2+} ions are within the standard deviation of MC-LR. Nevertheless, the median values of 1 and 14, respectively, highly differ which indicates a less stable binding between [β-D-Asp3,Dhb7]MC-RR and Mn^{2+} ions. The statistical analysis of the linear least-squares regression showed overall a similar trend compared to mean, median values and interquartile range (see SI Table 6). Nevertheless, the differences between less and non-toxic MC-congener to toxic MC-congeners were more easily determined and compared than with analysis of mean and median values.

3.4.2. *Qualitative analysis of binding*

To investigate the binding mechanism and differences in binding of different MC-congeners, the molecular interactions were analysed. MC-LR and MC-LF are highly toxic [29] and bind well to known interacting residues described by Fontanillo and Köhn [38] (see SI Figs. 7–9). The known residues of PPP1 important for interaction with MC congeners are pink sticks, while residues in close proximity (<4 Å) of MC congener are shown as green lines (see Figs. 8-11). When quantitatively analysing the distances between the respective protein residue and MC-congener atoms, the distance was low for both congeners and with fewer

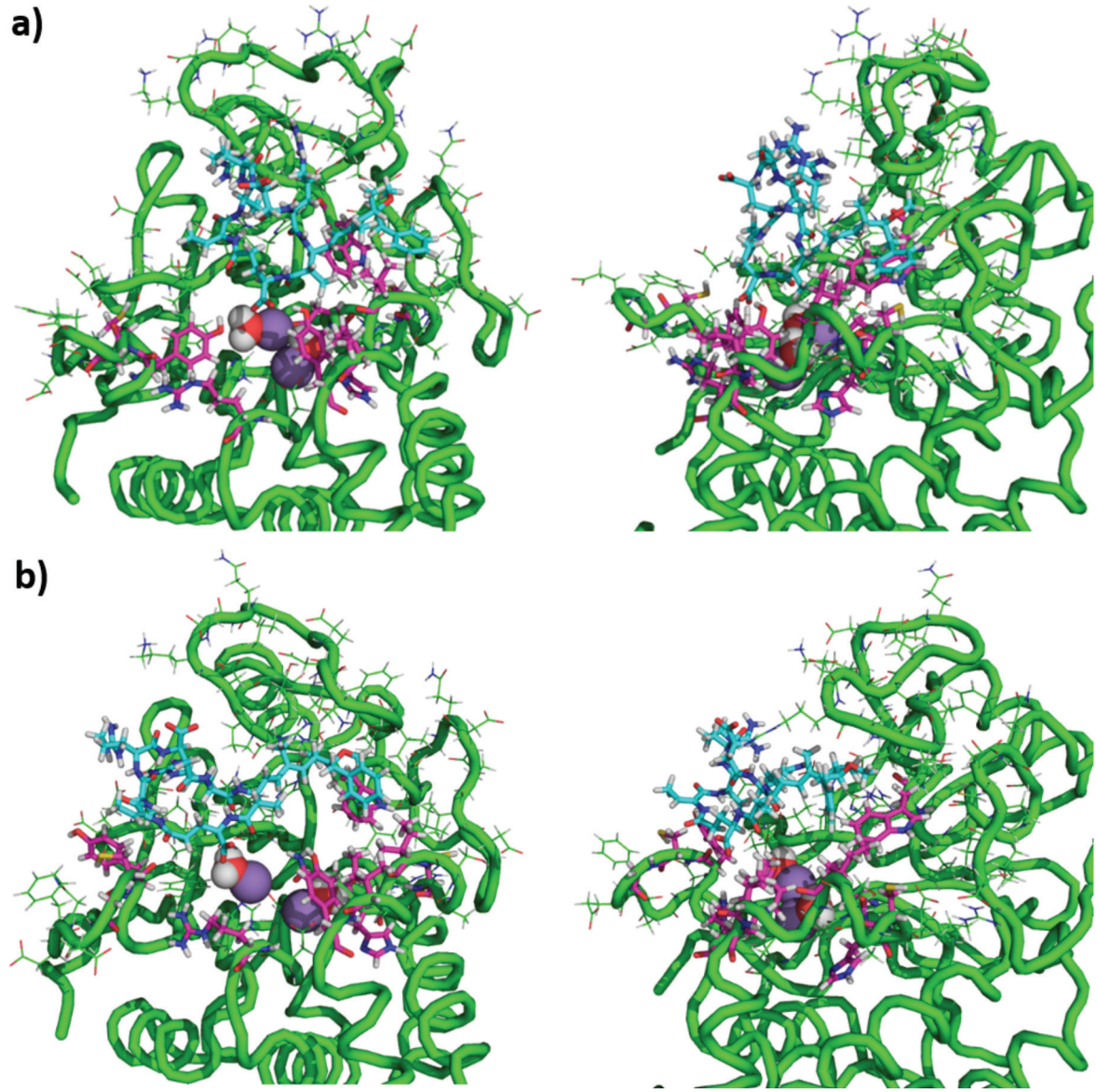

Fig. 11. Interaction of [β-D-Asp3,Dhb7]MC-RR (cyan) with PPP1 (green). Known interacting residues are displayed in pink, interacting residues as lines in green. Mn^{2+} and the active site water is shown as spheres. **a)** Are snapshots at the beginning (top and side view) and **b)** at the end (top and side view) of the third replicate.

fluctuations when compared to [*Enantio*-Adda5]MC-LF and [β-D-Asp3, Dhb7]MC-RR (data not shown).

[*Enantio*-Adda5]MC-LF, in contrast to MC-LF, is non-toxic [29], even though they only differ in four stereocenters of the Adda residue. This leads to a flip of the Adda residue when simulating the MC-congener in complex with PPP1 (see SI Fig. 10). In the beginning of the simulation (uncut trajectory, see Fig. 8), [Enantio-Adda5]MC-LF is coordinated in the binding site. During the third replicate [Enantio-Adda5]MC-LF started to move outside of the binding site. As the Adda residue was reported to be essential for binding to PPP1 [87], modification at the Adda stereocenters should result in a change of PPP1 interaction. Indeed, enantio-Adda cannot bind as stably to the respective protein residues (Cys127, Ile130, Ile133, Tyr134, Trp206) [38], and thus moves outside of the binding site (see Fig. 9a).

Interestingly, the MC-congener did not diffuse from the protein, but instead moved back to the binding site (see Fig. 10) and was flipped reverse into the PPP1 binding site (see Fig. 9b). Nevertheless, this was only observable in the last of all replicates.

[β-D-Asp3,Dhb7]MC-RR is modified at hyper-variable position 2, demethylated at position 3, and methylated at the unsaturated carbon atom at position 7 when compared to MC-LR and -LF (for a comparison of the structures see SI Fig. 11 and SI Fig. 12). These modifications lead to a more open backbone conformation (vide supra). The methyl group at position 3 appeared to change the backbone conformation of the ligand, probably leading to more stable binding. In contrast to [*Enantio*-Adda5]MC-LF, [β-D-Asp3,Dhb7]MC-RR did not move outside the binding site, but coordinated to the binding site in the simulation (see Fig. 11).

4. Conclusion

In conclusion we were able to demonstrate with MD simulation that different MC congeners bind differently to PPP1 and have different backbone conformations, whereas PPP1 structure is stable when simulated in solvent (as apo structure) or in complex with MC congeners. Evidence provided suggests that the MC-LR backbone can adopt to at least two conformations rather than a single one reported earlier and that these conformation changes may explain in part the tightness of PPP1 binding. For the first time we report backbone conformations of MC congeners. MC congeners can also adopt to a saddle-shaped

conformation, but do show different conformations than MC-LR. In our simulations we could show that less toxic and non-toxic MC congeners have a higher overlap and broader distribution of clusters for solvent and complex simulation in contrast to toxic MC congeners, indicating less stability of MC backbone structure. Since all computational studies so far focused solely on MC-LR, this study is a first step towards investigation of MC congener structures which were neglected so far. Nevertheless, further studies are necessary to investigate MC congener binding and toxicity towards PPP1 in closer detail and to simulate more MC congeners.

Availability of data and materials

The datasets and scripts supporting the conclusions of this article are available in the Zenodo repository:

1. https://doi.org/10.5281/zenodo.5017745 [90].
2. https://doi.org/10.5281/zenodo.5017839 [91].
3. https://doi.org/10.5281/zenodo.5017851 [92].

Funding

The authors gratefully acknowledge the Arthur-und-Aenne-Feindt foundation (Hamburg, Germany), and CHARM (Baden-Württemberg Wassernetzwerk) for financial support.

Authorship contribution statement

Sabrina Jaeger-Honz: Investigation, Software, Writing - Original Draft, Visualisation, Formal analysis. **Jahn Nitschke:** Investigation, Software, Writing - Original Draft. **Stefan Altaner:** Investigation, Writing - Review & Editing. **Karsten Klein:** Conceptualisation, Writing - Review & Editing. **Daniel R. Dietrich:** Conceptualisation, Supervision, Funding acquisition, Resources, Writing - Original Draft. **Falk Schreiber:** Conceptualisation, Supervision, Funding acquisition, Resources, Writing - Review & Editing.

Declaration of competing interest

The authors declare the following financial interests/personal relationships which may be considered as potential competing interests: Daniel R. Dietrich reports financial support was provided by Arthur-and-Aenne-Feindt Foundation (Hamburg, Germany). Stefan Altaner reports financial support was provided by Arthur-and-Aenne-Feindt Foundation (Hamburg, Germany). Daniel R. Dietrich reports financial support was provided by CHARM (Baden-Württemberg Wassernetzwerk).

Acknowledgements

The authors thank the Konstanz Research School Chemical Biology (KoRS-CB).

References

[1] D. De Figueiredo, U. Azeiteiro, S. Esteves, F. Gonçalves, M. Pereira, Microcystin-Producing blooms-A serious global public health issue, Ecotoxicol. Environ. Saf. 59 (2004) 151–163, https://doi.org/10.1016/j.ecoenv.2004.04.006.

[2] N. Bouaïcha, C.O. Miles, D.G. Beach, Z. Labidi, A. Djabri, N.Y. Benayache, T. Nguyen-Quang, Structural diversity, characterization and toxicology of microcystins, Toxins 11 (12) (2019), https://doi.org/10.3390/toxins11120714.

[3] K. Mez, K. Beattie, G. Codd, K. Hanselmann, B. Hauser, H. Naegeli, H. Preisig, Identification of a microcystin in benthic cyanobacteria linked to cattle deaths on alpine pastures in Switzerland, Eur. J. Phycol. 32 (2) (1997) 111–117, https://doi.org/10.1080/09670269710001737029.

[4] K. Frazier, B. Colvin, E. Styer, G. Hullinger, R. Garcia, Microcystin toxicosis in cattle due to overgrowth of blue-green algae, Vet. Hum. Toxicol. 40 (1) (1998) 23–24, place: United States.

[5] B. Puschner, F.D. Galey, B. Johnson, C.W. Dickie, M. Vondy, T. Francis, D. M. Holstege, Blue-green algae toxicosis in cattle, J. Am. Vet. Med. Assoc. 213 (11) (1998) 1605–1607, publisher: American Veterinary Medical Association.

[6] S.A. Wood, M.W. Heath, P.T. Holland, R. Munday, G.B. McGregor, K.G. Ryan, Identification of a benthic microcystin-producing filamentous cyanobacterium (Oscillatoriales) associated with a dog poisoning in New Zealand, Toxicon 55 (4) (2010) 897–903, https://doi.org/10.1016/j.toxicon.2009.12.019.

[7] D. van der Merwe, L. Sebbag, J.C. Nietfeld, M.T. Aubel, A. Foss, E. Carney, Investigation of a *Microcystis aeruginosa* cyanobacterial freshwater harmful algal bloom associated with acute microcystin toxicosis in a dog, J. Vet. Diagn. Invest. 24 (4) (2012) 679–687, https://doi.org/10.1177/1040638712445768.

[8] S.B. Hooser, V.R. Beasley, R.A. Lovell, W.W. Carmichael, W.M. Haschek, Toxicity of microcystin LR, a cyclic heptapeptide hepatotoxin from microcystis aeruginosa, to rats and mice, Vet. Pathol. 26 (3) (1989) 246–252, https://doi.org/10.1177/030098588902600309.

[9] C. MacKintosh, K.A. Beattie, S. Klumpp, P. Cohen, G.A. Codd, Cyanobacterial microcystin-LR is a potent and specific inhibitor of protein phosphatases 1 and 2A from both mammals and higher plants, FEBS (Fed. Eur. Biochem. Soc.) Lett. 264 (2) (1990) 187–192, https://doi.org/10.1016/0014-5793(90)80245-E.

[10] I.R. Falconer, M.D. Burch, D.A. Steffensen, M. Choice, O.R. Coverdale, Toxicity of the blue-green alga (cyanobacterium) Microcystis aeruginosa in drinking water to growing pigs, as an animal model for human injury and risk assessment, Environ. Toxicol. Water Qual. 9 (2) (1994) 131–139, https://doi.org/10.1002/tox.2530090209.

[11] G. Codd, S. Bell, K. Kaya, C. Ward, K. Beattie, J. Metcalf, Cyanobacterial toxins, exposure routes and human health, Eur. J. Phycol. 34 (4) (1999) 405–415, https://doi.org/10.1080/09670269910001736462, publisher: Taylor & Francis.

[12] Y. Li, J.-a. Chen, Q. Zhao, C. Pu, Z. Qiu, R. Zhang, W. Shu, A cross-sectional investigation of chronic exposure to microcystin in relationship to childhood liver damage in the three Gorges Reservoir region, China, Environ. Health Perspect. 119 (10) (2011) 1483–1488, https://doi.org/10.1289/ehp.1002412.

[13] A.E. Poste, R.E. Hecky, S.J. Guildford, Evaluating microcystin exposure risk through fish consumption, Environ. Sci. Technol. 45 (13) (2011) 5806–5811, https://doi.org/10.1021/es200285c.

[14] D.R. Dietrich, A. Fischer, C. Michel, S. Hoeger, Toxin mixture in cyanobacterial blooms – a critical comparison of reality with current procedures employed in human health risk assessment, in: H.K. Hudnell (Ed.), Cyanobacterial Harmful Algal Blooms: State of the Science and Research Needs, Springer, New York, 2008, pp. 885–912, https://doi.org/10.1007/978-0-387-75865-7_39.

[15] A. Heussner, L. Mazija, J. Fastner, D. Dietrich, Toxin content and cytotoxicity of algal dietary supplements, Toxicol. Appl. Pharmacol. 265 (2) (2012) 263–271, https://doi.org/10.1016/j.taap.2012.10.005.

[16] S.A. Wood, D.R. Dietrich, Quantitative assessment of aerosolized cyanobacterial toxins at two New Zealand lakes, J. Environ. Monit. 13 (6) (2011) 1617, https://doi.org/10.1039/c1em10102a.

[17] S. Pouria, A. de Andrade, J. Barbosa, R. Cavalcanti, V. Barreto, C. Ward, W. Preiser, G.K. Poon, G. Neild, G. Codd, Fatal microcystin intoxication in haemodialysis unit in Caruaru, Brazil, Lancet 352 (9121) (1998) 21–26, https://doi.org/10.1016/S0140-6736(97)12285-1.

[18] S.M.F.O. Azevedo, W.W. Carmichael, E.M. Jochimsen, K.L. Rinehart, S. Lau, G. R. Shaw, G.K. Eaglesham, Human intoxication by microcystins during renal dialysis treatment in Caruaru—Brazil, Toxicology 181–182 (2002) 441–446, https://doi.org/10.1016/S0300-483X(02)00491-2.

[19] M. Yuan, W.W. Carmichael, E.D. Hilborn, Microcystin analysis in human sera and liver from human fatalities in Caruaru, Brazil 1996, Toxicon 48 (6) (2006) 627–640, https://doi.org/10.1016/j.toxicon.2006.07.031.

[20] Y. Grosse, R. Baan, K. Straif, B. Secretan, F.E. Ghissassi, V. Cogliano, Carcinogenicity of nitrate, nitrite, and cyanobacterial peptide toxins, Lancet Oncol. 7 (8) (2006) 628–629, https://doi.org/10.1016/S1470-2045(06)70789-6.

[21] World Health Organization, Cyanobacterial Toxins: Microcystins, WHO/HEP/ECH/WSH/2020.6, 2020. https://apps.who.int/iris/handle/10665/338066. (Accessed 10 June 2021).

[22] J.K. Fawell, R.E. Mitchell, D.J. Everett, R.E. Hill, The toxicity of cyanobacterial toxins in the mouse: I microcystin-lr, Hum. Exp. Toxicol. 18 (3) (1999) 162–167, https://doi.org/10.1177/096032719901800305.

[23] A. Fischer, S.J. Hoeger, K. Stemmer, D.J. Feurstein, D. Knobeloch, A. Nussler, D. R. Dietrich, The role of organic anion transporting polypeptides (OATPs/SLCOs) in the toxicity of different microcystin congeners in vitro: a comparison of primary human hepatocytes and OATP-transfected HEK293 cells, Toxicol. Appl. Pharmacol. 245 (1) (2010) 9–20, https://doi.org/10.1016/j.taap.2010.02.006.

[24] W. Fischer, S. Altheimer, V. Cattori, P. Meier, D. Dietrich, B. Hagenbuch, Organic anion transporting polypeptides expressed in liver and brain mediate uptake of microcystin, Toxicol. Appl. Pharmacol. 203 (3) (2005) 257–263, https://doi.org/10.1016/j.taap.2004.08.012, risk Cyanobacterial Toxins: Occurance, Ecology, Detection, Toxicology and Health Effects Assessment.

[25] D. Feurstein, K. Holst, A. Fischer, D. Dietrich, OATP-associated uptake and toxicity of microcystins in primary Murine whole brain cells, Toxicol. Appl. Pharmacol. 234 (2009) 247–255, https://doi.org/10.1016/j.taap.2008.10.011.

[26] N.R. Saunders, R. Daneman, K.M. Dziegielewska, S.A. Liddelow, Transporters of the blood–brain and blood–CSF interfaces in development and in the adult, Mol.

Aspect. Med. 34 (2) (2013) 742–752, https://doi.org/10.1016/j.mam.2012.11.006.
[27] H. Liu, N. Yu, S. Lu, S. Ito, X. Zhang, B. Prasad, E. He, X. Lu, Y. Li, F. Wang, H. Xu, G. An, J.D. Unadkat, H. Kusuhara, Y. Sugiyama, J. Sahi, Solute carrier family of the organic anion-transporting polypeptides 1a2– madin-darby canine kidney II: a promising in vitro system to understand the role of organic anion-transporting polypeptide 1a2 in blood-brain barrier drug penetration, Drug Metab. Dispos. 43 (7) (2015) 1008–1018, https://doi.org/10.1124/dmd.115.064170.
[28] G. Kaur, R. Fahrner, V. Wittmann, B. Stieger, D.R. Dietrich, Human mrp2 exports mc-lr but not the glutathione conjugate, Chem. Biol. Interact. 311 (2019) 108761, https://doi.org/10.1016/j.cbi.2019.108761.
[29] S. Altaner, S. Jaeger, R. Fotler, I. Zemskov, V. Wittmann, F. Schreiber, D. Dietrich, Machine learning prediction of cyanobacterial toxin (microcystin) toxicodynamics in humans, ALTEX - Altern. Anim. Exp. 37 (1) (2020) 24–36, https://doi.org/10.14573/altex.1904031.
[30] C.J. Hastie, E.B. Borthwick, L.F. Morrison, G.A. Codd, P.T.W. Cohen, Inhibition of several protein phosphatases by a non-covalently interacting microcystin and a novel cyanobacterial peptide, nostocyclin, Biochim. Biophys. Acta Gen. Subj. 1726 (2) (2005) 187–193, https://doi.org/10.1016/j.bbagen.2005.06.005.
[31] S.J. Hoeger, D. Schmid, J.F. Blom, B. Ernst, D.R. Dietrich, Analytical and functional characterization of microcystins [asp3]mc-rr and [asp3,dhb7]mc-rr: consequences for risk assessment? Environ. Sci. Technol. 41 (7) (2007) 2609–2616, https://doi.org/10.1021/es062681p.
[32] F. Kondo, Y. Ikai, H. Oka, M. Okumura, N. Ishikawa, K. Harada, K. Matsuura, H. Murata, M. Suzuki, Formation, characterization, and toxicity of the glutathione and cysteine conjugates of toxic heptapeptide microcystins, Chem. Res. Toxicol. 5 (5) (1992) 591–596, https://doi.org/10.1021/tx00029a002.
[33] W.-s. Zong, S.-h. Zhang, Q. Wang, Y. Teng, Y.-z. Liu, Y.-g. Du, Evaluation of the direct and indirect regulation pathways of glutathione target to the hepatotoxicity of microcystin-LR, BioMed Res. Int. 2018 (2018) 1–8, https://doi.org/10.1155/2018/5672637.
[34] R.W. MacKintosh, K.N. Dalby, D.G. Campbell, P.T.W. Cohen, P. Cohen, C. MacKintosh, The cyanobacterial toxin microcystin binds covalently to cysteine-273 on protein phosphatase 1, FEBS (Fed. Eur. Biochem. Soc.) Lett. 371 (3) (1995) 236–240, https://doi.org/10.1016/0014-5793(95)00888-G.
[35] K. Mattila, A. Annila, T.T. Rantala, Metals Ions Mediate the Binding of Cyanobacterial Toxins to Human Protein Phosphatase 1-A Computational Study, Vol. A 351 of Acta Universitatis Ouluensis A, University of Oulu, 2000.
[36] B. Gulledge, J. Aggen, H. Eng, K. Sweimeh, A. Chamberlin, Microcystin analogues comprised only of Adda and a single additional amino acid retain moderate activity as PP1/PP2A inhibitors, Bioorg. Med. Chem. Lett 13 (2003) 2907–2911, https://doi.org/10.1016/S0960-894X(03)00588-2.
[37] M. Craig, H.A. Luu, T.L. McCready, C.F.B. Holmes, D. Williams, R.J. Andersen, Molecular mechanisms underlying the interaction of motuporin and microcystins with type-1 and type-2A protein phosphatases, Biochem. Cell. Biol. 74 (4) (1996) 569–578, https://doi.org/10.1139/o96-061.
[38] M. Fontanillo, M. Köhn, Microcystins: synthesis and structure–activity relationship studies toward pp1 and pp2a, Bioorg. Med. Chem. 26 (6) (2018) 1118–1126, https://doi.org/10.1016/j.bmc.2017.08.040.
[39] W. Carmichael, V. Beasley, D. Bunner, J. Eloff, I. Falconer, P. Gorham, K. Harada, T. Krishnamurthy, Y. Min-Juan, R. Moore, K. Rinehart, M. Runnegar, O. Skulberg, M. Watanabe, Naming of cyclic heptapeptide toxins of cyanobacteria (blue-green algae), Toxicon 26 (11) (1988) 971–973, https://doi.org/10.1016/0041-0101(88)90195-X, copyright: Copyright 2014 Elsevier B.V., All rights reserved.
[40] K.L. Rinehart, K. Harada, M. Namikoshi, C. Chen, C.A. Harvis, M.H.G. Munro, J. W. Blunt, P.E. Mulligan, V.R. Beasley, et al., Nodularin, microcystin, and the configuration of Adda, J. Am. Chem. Soc. 110 (25) (1988) 8557–8558, https://doi.org/10.1021/ja00233a049.
[41] E.M. Driggers, S.P. Hale, J. Lee, N.K. Terrett, The exploration of macrocycles for drug discovery — an underexploited structural class, Nat. Rev. Drug Discov. 7 (7) (2008) 608–624, https://doi.org/10.1038/nrd2590.
[42] C. Heinis, Tools and rules for macrocycles, Nat. Chem. Biol. 10 (9) (2014) 696–698, https://doi.org/10.1038/nchembio.1605.
[43] R. Hospital, Adam Goñi, M. Orozco, J. Gelpí, Molecular dynamics simulations: advances and applications, Comput. Biol. Chem. Adv. Appl. 10 (2015) 37, https://doi.org/10.2147/AABC.S70333.
[44] G.-B. Trogen, A. Annila, J. Eriksson, M. Kontteli, J. Meriluoto, I. Sethson, J. Zdunek, U. Edlund, Conformational studies of microcystin-lr using nmr spectroscopy and molecular dynamics calculations, Biochemistry 35 (10) (1996) 3197–3205, https://doi.org/10.1021/bi952368s.
[45] S.R. Pereira, V.M. Vasconcelos, A. Antunes, Computational study of the covalent bonding of microcystins to cysteine residues – a reaction involved in the inhibition of the ppp family of protein phosphatases, FEBS J. 280 (2) (2013) 674–680, https://doi.org/10.1111/j.1742-4658.2011.08454.x.
[46] A.L. Pochodylo, T.G. Aoki, L. Aristilde, Adsorption mechanisms of microcystin variant conformations at water–mineral interfaces: a molecular modeling investigation, J. Colloid Interface Sci. 480 (2016) 166–174, https://doi.org/10.1016/j.jcis.2016.07.016.
[47] A.L. Pochodylo, A.R. Klein, L. Aristilde, Metal-binding selectivity and coordination dynamics for cyanobacterial microcystins with zn, cu, fe, mg, and ca, Environ. Chem. Lett. 15 (4) (2017) 695–701, https://doi.org/10.1007/s10311-017-0639-x.
[48] W. Zong, Q. Wang, S. Zhang, Y. Teng, Y. Du, Regulation on the toxicity of microcystin-LR target to protein phosphatase 1 by biotransformation pathway: effectiveness and mechanism, Environ. Sci. Pollut. Control Ser. 25 (26) (2018) 26020–26029, https://doi.org/10.1007/s11356-018-2676-9.
[49] I. Zemskov, S. Altaner, D.R. Dietrich, V. Wittmann, Total synthesis of microcystin-LF and derivatives thereof, J. Org. Chem. 82 (7) (2017) 3680–3691, https://doi.org/10.1021/acs.joc.7b00175.
[50] F.C. Bernstein, T.F. Koetzle, G.J. Williams, E.F. Meyer, M.D. Brice, J.R. Rodgers, O. Kennard, T. Shimanouchi, M. Tasumi, The protein data bank: a computer-based archival file for macromolecular structures, J. Mol. Biol. 112 (3) (1977) 535–542, https://doi.org/10.1016/S0022-2836(77)80200-3.
[51] J. Goldberg, H. Huang, Y. Kwon, P. Greengard, A. Nairn, J. Kuriyan, Three-dimensional structure of the catalytic subunit of protein serine/threonine phosphatase-1, Nature 376 (6543) (1995) 745–753, https://doi.org/10.1038/376745a0.
[52] E.F. Pettersen, T.D. Goddard, C.C. Huang, G.S. Couch, D.M. Greenblatt, E.C. Meng, T.E. Ferrin, Ucsf chimera—a visualization system for exploratory research and analysis, J. Comput. Chem. 25 (13) (2004) 1605–1612, https://doi.org/10.1002/jcc.20084.
[53] MATLAB, Version 7.10.0 (R2016a), The MathWorks Inc., Natick, Massachusetts, 2016.
[54] G.M. Morris, R. Huey, W. Lindstrom, M.F. Sanner, R.K. Belew, D.S. Goodsell, A. J. Olson, Autodock4 and autodocktools4: automated docking with selective receptor flexibility, J. Comput. Chem. 30 (16) (2009) 2785–2791, https://doi.org/10.1002/jcc.21256.
[55] V.B. Chen, W.B. Arendall III, J.J. Headd, D.A. Keedy, R.M. Immormino, G.J. Kapral, L.W. Murray, J.S. Richardson, D.C. Richardson, MolProbity: all-atom structure validation for macromolecular crystallography, Acta Crystallogr. D 66 (1) (2010) 12–21, https://doi.org/10.1107/S0907444909042073.
[56] C.J. Williams, J.J. Headd, N.W. Moriarty, M.G. Prisant, L.L. Videau, L.N. Deis, V. Verma, D.A. Keedy, B.J. Hintze, V.B. Chen, S. Jain, S.M. Lewis, W.B. Arendall III, J. Snoeyink, P.D. Adams, S.C. Lovell, J.S. Richardson, D.C. Richardson, Molprobity: more and better reference data for improved all-atom structure validation, Protein Sci. 27 (1) (2018) 293–315, https://doi.org/10.1002/pro.3330.
[57] J.A. Maier, C. Martinez, K. Kasavajhala, L. Wickstrom, K.E. Hauser, C. Simmerling, ff14sb: improving the accuracy of protein side chain and backbone parameters from ff99sb, J. Chem. Theor. Comput. 11 (8) (2015) 3696–3713, https://doi.org/10.1021/acs.jctc.5b00255.
[58] C.W. Bock, A.K. Katz, G.D. Markham, J.P. Glusker, Manganese as a replacement for magnesium and zinc: functional comparison of the divalent ions, J. Am. Chem. Soc. 121 (32) (1999) 7360–7372, https://doi.org/10.1021/ja9906960.
[59] C.I. Bayly, P. Cieplak, W. Cornell, P.A. Kollman, A well-behaved electrostatic potential based method using charge restraints for deriving atomic charges: the resp model, J. Phys. Chem. 97 (40) (1993) 10269–10280, https://doi.org/10.1021/j100142a004.
[60] F.-Y. Dupradeau, A. Pigache, T. Zaffran, C. Savineau, R. Lelong, N. Grivel, D. Lelong, W. Rosanski, P. Cieplak, The r.e.d. tools: advances in resp and esp charge derivation and force field library building, Phys. Chem. Chem. Phys. 12 (2010) 7821–7839, https://doi.org/10.1039/C0CP00111B.
[61] E. Vanquelef, S. Simon, G. Marquant, E. Garcia, G. Klimerak, J.C. Delepine, P. Cieplak, F.-Y. Dupradeau, R.e.d. server: a web service for deriving resp and esp charges and building force field libraries for new molecules and molecular fragments, Nucleic Acids Res. 39 (2) (2011) W511–W517, https://doi.org/10.1093/nar/gkr288.
[62] F. Wang, J.-P. Becker, P. Cieplak, F.-Y. Dupradeau, R.E.D. Python: Object Oriented Programming for Amber Force Fields, Nov. 2013.
[63] M. Schmidt, K. Baldridge, J. Boatz, S. Elbert, M. Gordon, J. Jensen, S. Koseki, N. Matsunaga, K. Nguyen, S. Su, T. Windus, M. Dupuis, J. Montgomery, General atomic and molecular electronic structure system, J. Comput. Chem. 14 (11) (1993) 1347–1363, https://doi.org/10.1002/jcc.540141112.
[64] J. Wang, R.M. Wolf, J.W. Caldwell, P.A. Kollman, D.A. Case, Development and testing of a general amber force field, J. Comput. Chem. 25 (9) (2004) 1157–1174, https://doi.org/10.1002/jcc.20035.
[65] D. Case, R. Betz, D. Cerutti, T. Cheatham, T. Darden, R. Duke, T. Giese, H. Gohlke, A. Götz, N. Homeyer, S. Izadi, P. Janowski, J. Kaus, A. Kovalenko, T.-S. Lee, S. LeGrand, P. Li, C. Lin, T. Luchko, P. Kollman, Amber 16, University of california, San Francisco, 2016, https://doi.org/10.13140/RG.2.2.27958.70729, 04.
[66] M.R. Shirts, C. Klein, J.M. Swails, J. Yin, M.K. Gilson, D.L. Mobley, D.A. Case, E. D. Zhong, Lessons learned from comparing molecular dynamics engines on the SAMPL5 dataset, J. Comput. Aided Mol. Des. 31 (1) (2017) 147–161, https://doi.org/10.1007/s10822-016-9977-1.
[67] H. Bekker, H. Berendsen, E. Dijkstra, S. Achterop, R. Vondrumen, D. Vanderspoel, A. Sijbers, H. Keegstra, M. Renardus, Gromacs - a parallel computer for molecular-dynamics simulations, in: R. DeGroot, J. Nadrchal (Eds.), PHYSICS COMPUTING '92, World Scientific Publishing, 1993, pp. 252–256, 4th International Conference on Computational Physics (PC 92).
[68] M.J. Abraham, T. Murtola, R. Schulz, S. Páll, J.C. Smith, B. Hess, E. Lindahl, Gromacs: high performance molecular simulations through multi-level parallelism from laptops to supercomputers, SoftwareX 1–2 (2015) 19–25, https://doi.org/10.1016/j.softx.2015.06.001.
[69] W.L. Jorgensen, J. Chandrasekhar, J.D. Madura, R.W. Impey, M.L. Klein, Comparison of simple potential functions for simulating liquid water, J. Chem. Phys. 79 (2) (1983) 926–935, https://doi.org/10.1063/1.445869.
[70] S. Páll, B. Hess, A flexible algorithm for calculating pair interactions on simd architectures, Comput. Phys. Commun. 184 (12) (2013) 2641–2650, https://doi.org/10.1016/j.cpc.2013.06.003.
[71] B. Hess, H. Bekker, H.J.C. Berendsen, J.G.E.M. Fraaije, Lincs: a linear constraint solver for molecular simulations, J. Comput. Chem. 18 (12) (1997) 1463–1472, https://doi.org/10.1002/(SICI)1096-987X(199709)18:12<1463::AID-JCC4>3.0.CO;2-H.

[72] G. Bussi, D. Donadio, M. Parrinello, Canonical sampling through velocity rescaling, J. Chem. Phys. 126 (1) (2007), https://doi.org/10.1063/1.2408420, 014101.
[73] M. Parrinello, A. Rahman, Polymorphic transitions in single crystals: a new molecular dynamics method, J. Appl. Phys. 52 (12) (1981) 7182–7190, https://doi.org/10.1063/1.328693.
[74] M. Abraham, D. van der Spoel, E. Lindahl, B. Hess, the GROMACS development team, GROMACS User Manual Version 2016.4, 2017. www.gromacs.org.
[75] L. Capoferri, M. van Dijk, A.S. Rustenburg, T.A. Wassenaar, D.P. Kooi, E.A. Rifai, N. P.E. Vermeulen, D.P. Geerke, eTOX ALLIES: an automated pipeLine for linear interaction energy-based simulations, J. Cheminf. 9 (1) (2017) 58, https://doi.org/10.1186/s13321-017-0243-x.
[76] G. Van Rossum, F.L. Drake Jr., Python Reference Manual, Centrum voor Wiskunde en Informatica Amsterdam, 1995.
[77] C.R. Harris, K.J. Millman, S.J. van der Walt, R. Gommers, P. Virtanen, D. Cournapeau, E. Wieser, J. Taylor, S. Berg, N.J. Smith, R. Kern, M. Picus, S. Hoyer, M.H. van Kerkwijk, M. Brett, A. Haldane, J.F. del R'ıo, M. Wiebe, P. Peterson, P. G'erard-Marchant, K. Sheppard, T. Reddy, W. Weckesser, H. Abbasi, C. Gohlke, T.E. Oliphant, Array programming with NumPy, Nature 585 (7825) (2020) 357–362, https://doi.org/10.1038/s41586-020-2649-2.
[78] J.D. Hunter, Matplotlib: a 2d graphics environment, Comput. Sci. Eng. 9 (3) (2007) 90–95.
[79] S. Jaeger, S. Fulle, S. Turk, Mol2vec: unsupervised machine learning approach with chemical intuition, J. Chem. Inf. Model. 58 (1) (2018) 27–35, https://doi.org/10.1021/acs.jcim.7b00616.
[80] R. Biehl, Jscatter, a program for evaluation and analysis of experimental data, PLoS One 14 (6) (2019) 1–18, https://doi.org/10.1371/journal.pone.0218789.
[81] Grace - 2d Plotting Tool, 2008. https://plasma-gate.weizmann.ac.il/Grace/. (Accessed 10 June 2021).
[82] L. Schrödinger, Pymol - the Pymol Molecular Graphics System, Version 0.99, Schrödinger, Llc, November 2015.
[83] E. Jones, T. Oliphant, P. Peterson, et al., SciPy: Open Source Scientific Tools for Python, 2001. http://www.scipy.org/. (Accessed 10 June 2021).
[84] M.Y. Lobanov, N.S. Bogatyreva, O.V. Galzitskaya, Radius of gyration as an indicator of protein structure compactness, Mol. Biol. 42 (4) (2008) 623–628, https://doi.org/10.1134/S0026893308040195.
[85] B. Lee, F. Richards, The interpretation of protein structures: estimation of static accessibility, J. Mol. Biol. 55 (3) (1971), https://doi.org/10.1016/0022-2836(71)90324-X, 379–IN4.
[86] G.G. Maisuradze, A. Liwo, H.A. Scheraga, Principal component analysis for protein folding dynamics, J. Mol. Biol. 385 (1) (2009) 312–329, https://doi.org/10.1016/j.jmb.2008.10.018.
[87] K. Harada, K. Ogawa, K. Matsuura, H. Murata, M. Suzuki, M.F. Watanabe, Y. Itezono, N. Nakayama, Structural determination of geometrical isomers of microcystins lr and rr from cyanobacteria by two-dimensional nmr spectroscopic techniques, Chem. Res. Toxicol. 3 (5) (1990) 473–481, https://doi.org/10.1021/tx00017a014.
[88] G. Moorhead, R.W. MacKintosh, N. Morrice, T. Gallagher, C. MacKintosh, Purification of type 1 protein (serine/threonine) phosphatases by microcystin-sepharose affinity chromatography, FEBS (Fed. Eur. Biochem. Soc.) Lett. 356 (1) (1994) 46–50, https://doi.org/10.1016/0014-5793(94)01232-6.
[89] R.R. Stotts, M. Namikoshi, W.M. Haschek, K.L. Rinehart, W.W. Carmichael, A. M. Dahlem, V.R. Beasley, Structural modifications imparting reduced toxicity in microcystins from microcystis spp. Toxicon 31 (6) (1993) 783–789, https://doi.org/10.1016/0041-0101(93)90384-U.
[90] S. Jaeger-Honz, J. Nitschke, S. Altaner, K. Klein, D.R. Dietrich, F. Schreiber, Molecular Dynamics Simulation of Mc-Congeners in Complex with Ppp1-Replicate 1, Jun 2021, https://doi.org/10.5281/zenodo.5017745.
[91] S. Jaeger-Honz, J. Nitschke, S. Altaner, K. Klein, D.R. Dietrich, F. Schreiber, Molecular Dynamics Simulation of Mc-Congeners in Complex with Ppp1-Replicate 2, Jun 2021, https://doi.org/10.5281/zenodo.5017839.
[92] S. Jaeger-Honz, J. Nitschke, S. Altaner, K. Klein, D.R. Dietrich, F. Schreiber, Molecular Dynamics Simulation of Mc-Congeners in Complex with Ppp1-Replicate 3, Jun 2021, https://doi.org/10.5281/zenodo.5017851.